

A New Upwind Finite Volume Element Method for Convection-Diffusion-Reaction Problems on Quadrilateral Meshes

Ang Li¹, Hongtao Yang¹, Yulong Gao² and Yonghai Li^{1,*}

¹ School of Mathematics, Jilin University, Changchun 130012, Jilin, China.

² School of Mathematics, Hangzhou Normal University, Hangzhou 311121, China.

Received 14 July 2023; Accepted (in revised version) 29 October 2023

Abstract. This paper is devoted to constructing and analyzing a new upwind finite volume element method for anisotropic convection-diffusion-reaction problems on general quadrilateral meshes. We prove the coercivity, and establish the optimal error estimates in H^1 and L^2 norm respectively. The novelty is the discretization of convection term, which takes the two terms Taylor expansion. This scheme has not only optimal first-order accuracy in H^1 norm, but also optimal second-order accuracy in L^2 norm, both for dominant diffusion and dominant convection. Numerical experiments confirm the theoretical results.

AMS subject classifications: 65N08, 65N12

Key words: Convection-diffusion-reaction, upwind finite volume method, coercivity, optimal convergence rate in L^2 norm.

1 Introduction

In this paper, we consider the anisotropic convection-diffusion-reaction equation

$$\begin{cases} -\nabla \cdot (\kappa \nabla u - \mathbf{b} u) + c u = f, & \text{in } \Omega, \\ u = 0, & \text{on } \partial\Omega. \end{cases} \quad (1.1)$$

where $\Omega \subset \mathbb{R}^2$ is a polygonal domain with boundary $\partial\Omega$, the symmetric diffusion tensor $\kappa(x, y) = (\kappa_{ij}(x, y))_{i,j=1,2}$ satisfies the uniformly elliptic condition on Ω , i.e., there exist constants $0 < \mu_1 < \mu_2$, such that

$$\mu_1 |\xi|^2 \leq (\kappa(x, y) \xi, \xi) \leq \mu_2 |\xi|^2, \quad \forall \xi \in \mathbb{R}^2, \quad (1.2)$$

*Corresponding author. Email addresses: liang_0916@163.com (A. Li), yang_hungtao@163.com (H. Yang), flytoskygao@163.com (Y. Gao), yonghai@jlu.edu.cn (Y. Li)

$\mathbf{b}(x,y) = (b_1(x,y), b_2(x,y))^T$ is convection velocity, reaction term function $c(x,y) \geq c_{\min} > 0$, where c_{\min} is a constant, and the source term $f \in L^2(\Omega)$.

Convection-diffusion-reaction equation appears in various fields of engineering and science, such as fluid mechanics, petroleum reservoir simulation, groundwater prediction, and environmental protection. Many methods have been used to solve convection-diffusion equations including the finite difference method, the finite element method, and the finite volume method. It is well known that the straightforward application of these methods to the case of dominant convection may lead to spurious oscillations in the numerical solution. To avoid this drawback, many techniques have been developed, for example, streamline upwind Petrov-Galerkin method [1], residual-free bubbles approach [2], variational multiscale method [3], and upwind technique [4].

Due to the local conservation, the finite volume methods are widely used in numerical simulation for partial differential equations. According to the position of the unknowns on the meshes, the finite volume methods can usually be divided into cell-centered type and vertex-centered type. Cell-centered type of finite volume methods can be viewed as an extension of finite difference methods [5, 6], the construction of which is simple and flexible. Finite volume element method (FVEM) is a kind of special Petrov-Galerkin method, which belongs to the vertex-centered type [7]. FVEM has not only low-order element schemes [8–14], but also high-order element schemes [15–22]. Many first-order finite volume methods are constructed using upwind technique for convection-diffusion equations [7, 23–30].

Many researchers focus on developing finite volume methods for convection-diffusion equations, which have high-order accuracy and avoid spurious oscillations. For the cell-centered finite volume methods, many schemes are constructed by using slope limiter [31–35], or two terms Taylor expansion technique [36, 37]. In addition, a complete flux scheme (CFS) with second order accurate was developed on Cartesian grids with scalar diffusion [38]. Thereby, in order to deal with anisotropic diffusion tensors, Hanz Martin Cheng et al. establish a generalised complete flux scheme (GCFS) by combining CFS and the hybrid mimetic mixed method [39]. For FVEM, some schemes on rectangular meshes were proposed by constructing special dual meshes [40–42]. However, constructing special dual elements according to Peclet number needs additional computational cost. Under the standard dual partition, we hope to construct an upwind FVEM on general quadrilateral meshes with optimal convergence rate in L^2 norm.

In this paper, we construct a new upwind finite volume element method for the anisotropic convection-diffusion-reaction problems on general quadrilateral meshes. The trial space is taken as bilinear element space on quadrilateral meshes, and test space is taken as a piecewise constant function space on dual partition. We discrete the diffusion term by standard bilinear element finite volume method, which allows us to handle anisotropic diffusion tensors. Especially, the key ingredient is the discretization of the convection term, inspired by the idea in [37], we take the two terms of Taylor expansion of the solution at the upstream point to replace the solution on dual element boundary. Compared to the standard upwind scheme whose L^2 convergence rate is $\mathcal{O}(h)$, the

L^2 convergence rate of our scheme is $\mathcal{O}(h^2)$. Under some assumptions on quadrilateral meshes and the regularity of exact solution, we carry out the stability of the scheme, and prove the optimal convergence rate in H^1 norm and L^2 norm respectively, where the L^2 error estimate is based on superconvergence result. A series of numerical experiments are presented to confirm the theoretical results.

The outline of this paper is as follows. In Section 2, we propose a new upwind finite volume element method for convection-diffusion-reaction problems on quadrilateral meshes. The coercivity is established in Section 3. In Section 4, we carry out the optimal error estimate in H^1 norm and L^2 norm. A series of numerical results are presented in Section 5. Finally, the conclusions are given in Section 6.

2 A new upwind finite volume element method on quadrilateral meshes

In this section, we construct a new upwind finite volume element method for problem (1.1) on quadrilateral meshes.

Let $\mathcal{T}_h = \{K\}$ be a quadrilateral partition of Ω , where K is any quadrilateral element. Let ρ_K be the diameter of the largest disk contained in element K , h_K be the diameter of element K , $\Theta(K)$ be the set of interior angles of K , and h be the largest diameter of all quadrilateral elements. We call \mathcal{T}_h is regular, if there exist constants C and $\theta_0 > 0$, for any element $K \in \mathcal{T}_h$ and any $\theta \in \Theta(K)$, such that $\frac{h_K}{\rho_K} \leq C$ and $\theta_0 \leq \theta \leq \pi - \theta_0$. And we call \mathcal{T}_h is quasi-uniform, if there exists a constant $C > 0$, such that $Ch^2 \leq S_K \leq h^2, K \in \mathcal{T}_h$. Denote the set of the nodes of \mathcal{T}_h by \mathcal{P}_h .

In order to define the trial space U_h , we take the unit square $\hat{K} = [0,1]^2$ on the (ξ, η) plane as a reference element. For any convex quadrilateral element K , there exists a unique invertible bilinear transformation F_K which maps \hat{K} onto K

$$F_K : \begin{cases} x = x_1 + \alpha_1 \xi + \alpha_2 \eta + \alpha_3 \xi \eta, \\ y = y_1 + \beta_1 \xi + \beta_2 \eta + \beta_3 \xi \eta, \end{cases} \quad (2.1)$$

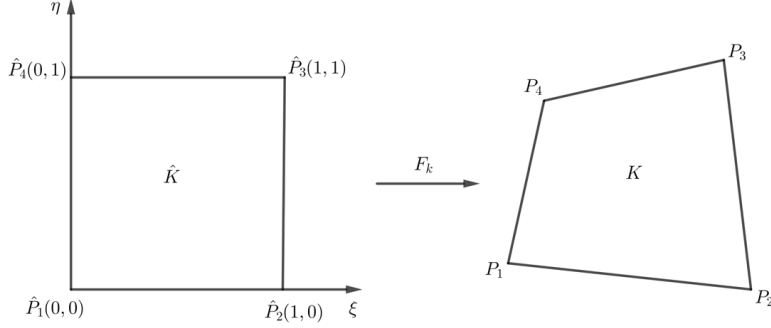
where

$$\alpha_1 = x_2 - x_1, \quad \alpha_2 = x_4 - x_1, \quad \alpha_3 = x_3 - x_4 - x_2 + x_1, \quad (2.2)$$

$$\beta_1 = y_2 - y_1, \quad \beta_2 = y_4 - y_1, \quad \beta_3 = y_3 - y_4 - y_2 + y_1, \quad (2.3)$$

and (x_i, y_i) , $i = 1, 2, 3, 4$, are the coordinates of the vertices P_i of K , see Fig. 1. Denote the Jacobi matrix of transformation F_K by J_K , and the determinant of J_K by J_K , then

$$J_K(\xi, \eta) = \begin{pmatrix} \frac{\partial x}{\partial \xi} & \frac{\partial x}{\partial \eta} \\ \frac{\partial y}{\partial \xi} & \frac{\partial y}{\partial \eta} \end{pmatrix} = \begin{pmatrix} \alpha_1 + \alpha_3 \eta & \alpha_2 + \alpha_3 \xi \\ \beta_1 + \beta_3 \eta & \beta_2 + \beta_3 \xi \end{pmatrix}, \quad (2.4)$$

Figure 1: Bilinear transformation F_K .

and according to the differentiation of inverse function, we have

$$\begin{pmatrix} \frac{\partial \xi}{\partial x} & \frac{\partial \xi}{\partial y} \\ \frac{\partial \eta}{\partial x} & \frac{\partial \eta}{\partial y} \end{pmatrix} = \mathcal{J}_K^{-1}(\xi, \eta) = \frac{1}{J_K} \begin{pmatrix} \beta_2 + \beta_3 \xi & -(\alpha_2 + \alpha_3 \xi) \\ -(\beta_1 + \beta_3 \eta) & \alpha_1 + \alpha_3 \eta \end{pmatrix}. \quad (2.5)$$

Let $U_h(\hat{K})$ be the standard bilinear polynomial space on \hat{K} , and then we define the trial space as

$$U_h = \left\{ u_h \in C(\bar{\Omega}) : u_h|_K = \hat{u}_h \circ F_K^{-1}, \hat{u}_h \in U_h(\hat{K}), \forall K \in \mathcal{T}_h, u_h|_{\partial\Omega} = 0 \right\}, \quad (2.6)$$

where $u_h|_K = \hat{u}_h \circ F_K^{-1}$ represents the compound function of \hat{u}_h and the inverse transformation F_K^{-1} . Then for any $u_h \in U_h$, u_h restricted on K can be denoted as

$$u_h|_K = u_1(1-\xi)(1-\eta) + u_2\xi(1-\eta) + u_3\xi\eta + u_4(1-\xi)\eta, \quad (2.7)$$

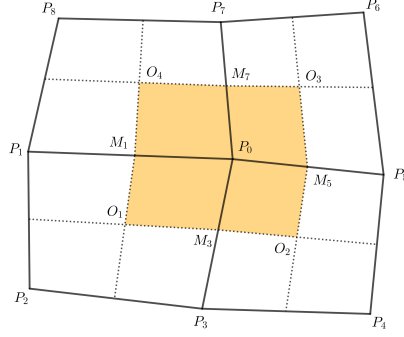
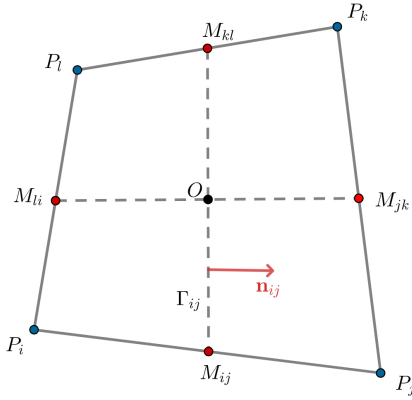
where $u_i = u_h(P_i)$ ($i=1,2,3,4$).

Then we construct the dual partition \mathcal{T}_h^* corresponding to primary partition \mathcal{T}_h . Connect midpoints of opposite edges of quadrilateral element K , and the two line segments intersect at the averaging center. As shown in Fig. 2, the dual element $K_{P_0}^*$ surrounding P_0 is a polygon formed by successively connecting points $\{O_1, M_3, O_2, M_5, O_3, M_7, O_4, M_1, O_1\}$, where O_i are the averaging centers, and M_i are the edge midpoints. Then all the dual elements constitute the dual partition $\mathcal{T}_h^* = \{K_P^*, P \in \mathcal{P}_h\}$. Let \mathcal{E} be the set of boundary line segments of all dual elements. Furthermore, we define the test space as a piecewise constant space on dual meshes

$$V_h = \left\{ v_h \in L^2(\bar{\Omega}) : v_h|_{K_P^*} = \text{constant}, \forall K_P^* \in \mathcal{T}_h^*, v_h|_{K_{P_0}^*} = 0, \forall P_0 \in \partial\Omega \right\}. \quad (2.8)$$

Let Π_h^* be the interpolation operator from U_h to V_h , which is defined as

$$\Pi_h^* u_h = \sum_{P \in \mathcal{P}_h} u_h(P) \psi_P, \quad (2.9)$$

Figure 2: Dual element surrounding P_0 .Figure 3: Element K .

where ψ_P is the characteristic functions on K_P^* .

In order to construct the upwind finite volume element method, we first define the bilinear form with upwind idea for convection term. Let E be the common edge of two adjacent elements K_1 and K_2 in \mathcal{T}_h . The average gradient at any point $(\tilde{x}, \tilde{y}) \in E$ is defined as

$$\bar{\nabla}v(\tilde{x}, \tilde{y}) = \frac{1}{2} \left((\nabla v|_{K_1})(\tilde{x}, \tilde{y}) + (\nabla v|_{K_2})(\tilde{x}, \tilde{y}) \right). \quad (2.10)$$

Especially, if $v \in C^1(K_1 \cup K_2)$, then $\bar{\nabla}v = \nabla v$.

Define $\Gamma_{ij} \subset K$ is the common boundary edge of two adjacent dual elements $K_{P_i}^*$ and $K_{P_j}^*$, see Fig. 3. Without losing generality, for any point $\forall (x, y) \in \Gamma_{ij}$, the corresponding coordinates on reference plane (ξ, η) is $(\frac{1}{2}, \eta) = F_K^{-1}(x, y)$, $\eta \in (0, \frac{1}{2})$. Then we define the

upstream point (x^{up}, y^{up}) as

$$(x^{up}, y^{up}) = \begin{cases} F_K(0, \eta), & \text{if } \int_{\Gamma_{ij}} \mathbf{b} \cdot \mathbf{n}_{ij} ds \geq 0, \\ F_K(1, \eta), & \text{if } \int_{\Gamma_{ij}} \mathbf{b} \cdot \mathbf{n}_{ij} ds < 0, \end{cases} \quad (2.11)$$

where \mathbf{n}_{ij} denotes the unit outer normal vector of $\partial K_{P_i}^*$. And we call K^{up} the upstream element of K corresponding to Γ_{ij} , if $(x^{up}, y^{up}) \in (\partial K \cap \partial K^{up})$. Similar to [37], we use two terms of Taylor expansion u^{up} to approximate u and we define the upwind approximation u^{up} for u as follow,

$$u^{up} = u(x^{up}, y^{up}) + \mathbf{r} \cdot \bar{\nabla} u(x^{up}, y^{up}), \quad (2.12)$$

where $\mathbf{r} = (x - x^{up}, y - y^{up})$. We would like to point out that, in [37], the gradient is approximated by the difference quotient of the auxiliary unknowns, for our scheme, the gradient is defined by the average gradient (2.10).

Especially, for $(x^{up}, y^{up}) \in \partial \Omega$, we take $\bar{\nabla} u(x^{up}, y^{up}) = (\nabla u|_K)(x^{up}, y^{up})$, where $(x^{up}, y^{up}) \in K$.

Then the bilinear form for convection term is defined as

$$b_h(u_h, v_h) = \sum_{K_P^* \in \mathcal{T}_h^*} \int_{\partial K_P^*} (\mathbf{b} \cdot \mathbf{n}) u_h^{up} v_h ds, \quad \forall u_h \in U_h, \quad \forall v_h \in V_h. \quad (2.13)$$

The bilinear form for the diffusion term is defined as

$$a(u_h, v_h) = \sum_{K_P^* \in \mathcal{T}_h^*} - \int_{\partial K_P^*} (\kappa \nabla u_h) \cdot \mathbf{n} v_h ds, \quad \forall u_h \in U_h, \quad \forall v_h \in V_h. \quad (2.14)$$

The bilinear form for the reaction term is defined as

$$c(u_h, v_h) = \sum_{K_P^* \in \mathcal{T}_h^*} \iint_{K_P^*} c u_h v_h dx dy, \quad \forall u_h \in U_h, \quad \forall v_h \in V_h. \quad (2.15)$$

Furthermore, the L^2 inner product for the source term is defined as

$$(f, v_h) = \sum_{K_P^* \in \mathcal{T}_h^*} \iint_{K_P^*} f v_h dx dy, \quad \forall v_h \in V_h. \quad (2.16)$$

The upwind finite volume element method for convection-diffusion-reaction equation (1.1) is to find $u_h \in U_h$, such that

$$A(u_h, v_h) = a(u_h, v_h) + b_h(u_h, v_h) + c(u_h, v_h) = (f, v_h), \quad \forall v_h \in V_h. \quad (2.17)$$

In addition, the exact solution satisfies the variational equation

$$a(u, v_h) + b(u, v_h) + c(u, v_h) = (f, v_h), \quad \forall v_h \in V_h, \quad (2.18)$$

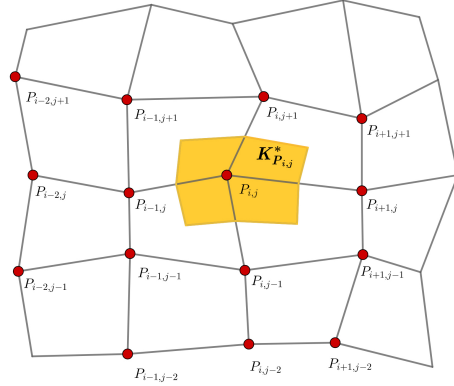


Figure 4: Non-zero element stencil.

where

$$b(u, v_h) = \sum_{K_p^* \in \mathcal{T}_h^*} \int_{\partial K_p^*} (\mathbf{b} \cdot \mathbf{n}) u v_h ds, \quad (2.19)$$

and the definition of $a(u, v_h)$, $c(u, v_h)$ and (f, v_h) are the same as (2.14), (2.15) and (2.16) respectively.

Remark 2.1. Since the discretization of convection term needs to use the information of upstream element, our scheme has more non-zero elements than the standard bilinear element finite volume method. On structured quadrilateral meshes, the stencil of our scheme has 15 points, while the stencil of standard bilinear element finite volume method has 9 points. Fig. 4 shows the stencil of our scheme on dual element $K_{P_{i,j}}^*$, when $b_1, b_2 \geq 0$.

Remark 2.2. Based on the similar idea, we can extend our scheme to hexahedral meshes in three-dimensional. The theoretical analysis is similar to quadrilateral meshes. Numerical experiment confirms that our scheme has optimal convergence order on hexahedral meshes, see Example 5.6 in Section 5.

3 Coercivity

In this section, we prove the coercivity of the upwind finite volume element method. Firstly, we introduce the discrete semi-norm

$$|u_h|_{1,h} = \left(\sum_{K \in \mathcal{T}_h} |u_h|_{1,K,h}^2 \right)^{\frac{1}{2}}, \quad \forall u_h \in U_h, \quad (3.1)$$

where

$$|u_h|_{1,K,h}^2 = (u_2 - u_1)^2 + (u_3 - u_2)^2 + (u_3 - u_4)^2 + (u_4 - u_1)^2. \quad (3.2)$$

On the basis of paper [10], $|u_h|_{1,h}$ and $|u_h|_1$ have the following equivalence.

Lemma 3.1. *Assume that \mathcal{T}_h is regular, then the discrete semi-norms $|u_h|_{1,h}$ and $|u_h|_1$ are equivalent over U_h , that is, there exist positive constants C_1 and C_2 independent of h , such that*

$$C_1|u_h|_{1,h} \leq |u_h|_1 \leq C_2|u_h|_{1,h}, \quad \forall u_h \in U_h. \quad (3.3)$$

According to papers [10] and [18], the diffusion term satisfies the coercivity, when the meshes satisfy the $h^{1+\gamma}$ -parallelogram condition for any $\gamma \in (0,1]$, that is, if any element $K = \square P_1 P_2 P_3 P_4 \in \mathcal{T}_h$ satisfies $|\overrightarrow{P_1 P_2} + \overrightarrow{P_3 P_4}| \leq Ch^{1+\gamma}$, see Fig. 1.

Lemma 3.2. *Suppose that \mathcal{T}_h is a regular and $h^{1+\gamma}$ -parallelogram partition ($0 < \gamma \leq 1$), there holds that,*

$$a(u_h, \Pi_h^* u_h) \geq C_3 \mu_1 |u_h|_1^2, \quad \forall u_h \in U_h, \quad (3.4)$$

where C_3 is a positive constant dependent of γ . The proof of (3.4) can be found in [10] and [18].

According to [14] and [21], the reaction term satisfies following lemma.

Lemma 3.3. *Assume that \mathcal{T}_h is a regular and $h^{1+\gamma}$ -parallelogram partition ($0 < \gamma \leq 1$), there exists a constant C_4 , such that*

$$c(u_h, \Pi_h^* u_h) \geq C_4 c_{\min} \|u_h\|_0^2, \quad \forall u_h \in U_h, \quad (3.5)$$

where constant C_4 depends on γ .

Now we prove the positive definiteness of bilinear form $A(u_h, \Pi_h^* u_h)$.

Theorem 3.1 (Coercivity). *Assume that \mathcal{T}_h is a quasi-uniform and $h^{1+\gamma}$ -parallelogram partition ($0 < \gamma \leq 1$), if $C_4 c_{\min} - \frac{1}{2} |\nabla \cdot \mathbf{b}|_\infty \geq 0$, where C_4 is the constant in (3.5), then for any $u_h \in U_h$, there exists a constant C for h small enough, such that*

$$A(u_h, \Pi_h^* u_h) = a(u_h, \Pi_h^* u_h) + b_h(u_h, \Pi_h^* u_h) + c(u_h, \Pi_h^* u_h) \geq C \|u_h\|_1^2, \quad (3.6)$$

where constant C depends on γ , μ_1 , \mathbf{b} and c_{\min} .

Proof. Firstly, we discuss the bilinear form of convection term $b_h(u_h, \Pi_h^* u_h)$.

$$\begin{aligned}
& b_h(u_h, \Pi_h^* u_h) \\
&= \sum_{K_P^* \in \mathcal{T}_h^*} \int_{\partial K_P^*} (\mathbf{b} \cdot \mathbf{n}) u_h^{up} \Pi_h^* u_h ds \\
&= \sum_{K_P^* \in \mathcal{T}_h^*} \int_{\partial K_P^*} (\mathbf{b} \cdot \mathbf{n}) \left(u_h(x^{up}, y^{up}) + \mathbf{r} \cdot \bar{\nabla} u_h(x^{up}, y^{up}) \right) \Pi_h^* u_h ds \\
&= \sum_{K_P^* \in \mathcal{T}_h^*} \int_{\partial K_P^*} (\mathbf{b} \cdot \mathbf{n}) \left((u_h(x^{up}, y^{up}) + \mathbf{r} \cdot \nabla u_h|_K(x^{up}, y^{up})) \right. \\
&\quad \left. + \frac{\mathbf{r}}{2} \cdot (\nabla u_h|_{K^{up}}(x^{up}, y^{up}) - \nabla u_h|_K(x^{up}, y^{up})) \right) \Pi_h^* u_h ds \\
&= \sum_{K_P^* \in \mathcal{T}_h^*} \int_{\partial K_P^*} (\mathbf{b} \cdot \mathbf{n}) u_h \Pi_h^* u_h ds \\
&\quad + \sum_{K_P^* \in \mathcal{T}_h^*} \int_{\partial K_P^*} (\mathbf{b} \cdot \mathbf{n}) \frac{\mathbf{r}}{2} \cdot (\nabla u_h|_{K^{up}}(x^{up}, y^{up}) - \nabla u_h|_K(x^{up}, y^{up})) \Pi_h^* u_h ds \\
&= B_1 + B_2,
\end{aligned} \tag{3.7}$$

where $\mathbf{r} = (x - x^{up}, y - y^{up})$. By calculation, we have

$$\int_{\Omega} \nabla \cdot (\mathbf{b} u_h) u_h dx dy = \frac{1}{2} \int_{\Omega} (\nabla \cdot \mathbf{b}) u_h^2 dx dy. \tag{3.8}$$

For the first part of (3.7), we have

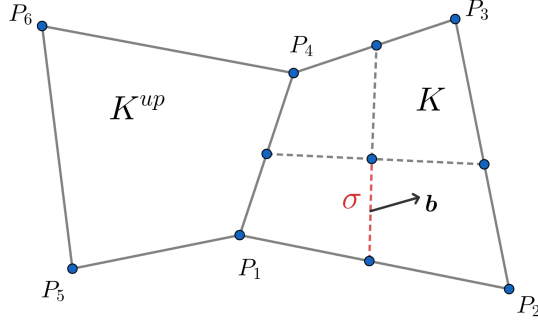
$$\begin{aligned}
B_1 &= \sum_{K_P^* \in \mathcal{T}_h^*} \int_{\partial K_P^*} (\mathbf{b} \cdot \mathbf{n}) u_h \Pi_h^* u_h ds = \sum_{K_P^* \in \mathcal{T}_h^*} \int_{K_P^*} \nabla \cdot (\mathbf{b} u_h) \Pi_h^* u_h dx dy \\
&= \int_{\Omega} \nabla \cdot (\mathbf{b} u_h) \Pi_h^* u_h dx dy.
\end{aligned} \tag{3.9}$$

Based on (3.8)-(3.9), then

$$\begin{aligned}
B_1 &= \int_{\Omega} \nabla \cdot (\mathbf{b} u_h) \Pi_h^* u_h dx dy - \int_{\Omega} \nabla \cdot (\mathbf{b} u_h) u_h dx dy + \int_{\Omega} \nabla \cdot (\mathbf{b} u_h) u_h dx dy \\
&= \int_{\Omega} \nabla \cdot (\mathbf{b} u_h) (\Pi_h^* u_h - u_h) dx dy + \frac{1}{2} \int_{\Omega} (\nabla \cdot \mathbf{b}) u_h^2 dx dy \\
&= \int_{\Omega} ((\nabla \cdot \mathbf{b}) u_h + \mathbf{b} \cdot \nabla u_h) (\Pi_h^* u_h - u_h) dx dy + \frac{1}{2} \int_{\Omega} (\nabla \cdot \mathbf{b}) u_h^2 dx dy.
\end{aligned} \tag{3.10}$$

Utilizing Cauchy-Schwarz inequality and Poincare inequality, we obtain

$$\begin{aligned}
|B_1| &\leq \left(|\nabla \cdot \mathbf{b}|_{\infty} \|u_h\|_0 + |\mathbf{b}|_{\infty} |u_h|_1 \right) \|\Pi_h^* u_h - u_h\|_0 + \frac{1}{2} |\nabla \cdot \mathbf{b}|_{\infty} \|u_h\|_0^2 \\
&\leq C h \left(|\mathbf{b}|_{\infty} + |\nabla \cdot \mathbf{b}|_{\infty} \right) |u_h|_1^2 + \frac{1}{2} |\nabla \cdot \mathbf{b}|_{\infty} \|u_h\|_0^2,
\end{aligned} \tag{3.11}$$

Figure 5: Element K and upstream element K^{up} .

where $|\mathbf{b}|_\infty = \max_{\Omega}(|b_1|, |b_2|)$, and $|\nabla \cdot \mathbf{b}|_\infty = \max_{\Omega}(|\nabla \cdot \mathbf{b}|)$.

For the second part of (3.7), we get

$$\begin{aligned} B_2 &= \sum_{K_P^* \in \mathcal{T}_h^*} \int_{\partial K_P^*} (\mathbf{b} \cdot \mathbf{n}) \frac{\mathbf{r}}{2} \cdot (\nabla u_h|_{K^{up}}(x^{up}, y^{up}) - \nabla u_h|_K(x^{up}, y^{up})) \Pi_h^* u_h ds \\ &= \sum_{\sigma \in \mathcal{E}} \int_{\sigma} (\mathbf{b} \cdot \mathbf{n}) \frac{\mathbf{r}}{2} \cdot (\nabla u_h|_{K^{up}}(x^{up}, y^{up}) - \nabla u_h|_K(x^{up}, y^{up})) [\Pi_h^* u_h] ds, \end{aligned} \quad (3.12)$$

where $[\Pi_h^* u_h] = \Pi_h^* u_h|_{K_1^*} - \Pi_h^* u_h|_{K_2^*}$ is the jump of $\Pi_h^* u_h$ on edge σ , K_1^* and K_2^* are adjacent dual elements. For any $\sigma \in \mathcal{E}$, without losing generality, we assume $\int_{\sigma} \mathbf{b} \cdot \mathbf{n} ds \geq 0$, see Fig. 5, then we have

$$\begin{aligned} &\left| \int_{\sigma} (\mathbf{b} \cdot \mathbf{n}) \frac{\mathbf{r}}{2} \cdot (\nabla u_h|_{K^{up}}(x^{up}, y^{up}) - \nabla u_h|_K(x^{up}, y^{up})) [\Pi_h^* u_h] ds \right| \\ &\leq C |\mathbf{b}|_\infty |u_h|_{1,K} \int_0^{\frac{1}{2}} \left| \mathbf{r}\left(\frac{1}{2}, \eta\right) \cdot \left(\mathcal{J}_{K^{up}}^{-1}(1, \eta) \hat{\nabla} u_h|_{K^{up}}(1, \eta) \right. \right. \\ &\quad \left. \left. - \mathcal{J}_K^{-1}(0, \eta) \hat{\nabla} u_h|_K(0, \eta) \right) \left(\left| \frac{\partial y}{\partial \eta} \right| + \left| \frac{\partial x}{\partial \eta} \right| \right) \right| d\eta \quad (3.13) \\ &\leq Ch^2 |\mathbf{b}|_\infty |u_h|_{1,K} \left(\int_0^{\frac{1}{2}} \left| \mathcal{J}_{K^{up}}^{-1}(1, \eta) \hat{\nabla} u_h|_{K^{up}}(1, \eta) \right| d\eta + \int_0^{\frac{1}{2}} \left| \mathcal{J}_K^{-1}(0, \eta) \hat{\nabla} u_h|_K(0, \eta) \right| d\eta \right) \\ &\leq Ch^2 |\mathbf{b}|_\infty |u_h|_{1,K} \left(\|\mathcal{J}_{K^{up}}^{-1}\|_{F,\infty} \int_0^{\frac{1}{2}} |\hat{\nabla} u_h|_{K^{up}}(1, \eta) d\eta + \|\mathcal{J}_K^{-1}\|_{F,\infty} \int_0^{\frac{1}{2}} |\hat{\nabla} u_h|_K(0, \eta) d\eta \right), \end{aligned}$$

where $\|\mathcal{J}_K^{-1}\|_{F,\infty} = \max_{(\xi, \eta) \in \mathcal{K}} \|\mathcal{J}_K^{-1}(\xi, \eta)\|_F$, $\hat{\nabla} u_h = (\frac{\partial u_h}{\partial \xi}, \frac{\partial u_h}{\partial \eta})^T$, and here we use $\left| \frac{\partial y}{\partial \eta} \right| \leq Ch$, $\left| \frac{\partial x}{\partial \eta} \right| \leq Ch$.

According to [13], there holds

$$\|\mathcal{J}_K^{-1}\|_{F,\infty} \leq C_K \frac{1}{h_K}, \quad \|\mathcal{J}_{K^{up}}^{-1}\|_{F,\infty} \leq C_{K^{up}} \frac{1}{h_{K^{up}}}. \quad (3.14)$$

By calculation, we obtain

$$\begin{aligned} \int_0^{\frac{1}{2}} |\hat{\nabla} u_h|_K(0, \eta) |d\eta| &= \int_0^{\frac{1}{2}} \left(((u_2 - u_1) + (u_3 - u_4 - u_2 + u_1)\eta)^2 + (u_4 - u_1)^2 \right)^{\frac{1}{2}} d\eta \\ &\leq C((u_2 - u_1)^2 + (u_3 - u_4)^2 + (u_4 - u_1)^2)^{\frac{1}{2}} \\ &\leq C|u_h|_{1,K}. \end{aligned} \quad (3.15)$$

Similarly,

$$\int_0^{\frac{1}{2}} |\hat{\nabla} u_h|_{K^{up}}(1, \eta) |d\eta| \leq C|u_h|_{1,K^{up}}. \quad (3.16)$$

Since \mathcal{T}_h is quasi-uniform, based on (3.12)-(3.16) and Cauchy-Schwarz inequality, we get

$$\begin{aligned} |B_2| &\leq Ch|\mathbf{b}|_\infty \sum_{\sigma \in \mathcal{E}} |u_h|_{1,K} (|u_h|_{1,K} + |u_h|_{1,K^{up}}) \\ &\leq Ch|\mathbf{b}|_\infty |u_h|_1^2. \end{aligned} \quad (3.17)$$

By (3.11) and (3.17), we obtain

$$|b_h(u_h, \Pi_h^* u_h)| \leq C_5 h (|\mathbf{b}|_\infty + |\nabla \cdot \mathbf{b}|_\infty) |u_h|_1^2 + \frac{1}{2} |\nabla \cdot \mathbf{b}|_\infty |u_h|_0^2. \quad (3.18)$$

If $C_3 \mu_1 - C_5 h (|\mathbf{b}|_\infty + |\nabla \cdot \mathbf{b}|_\infty) > 0$ and $C_4 c_{\min} - \frac{1}{2} |\nabla \cdot \mathbf{b}|_\infty \geq 0$, we have the following positive definiteness,

$$\begin{aligned} A(u_h, \Pi_h^* u_h) &= a(u_h, \Pi_h^* u_h) + b_h(u_h, \Pi_h^* u_h) + c(u_h, \Pi_h^* u_h) \\ &\geq \left(C_3 \mu_1 - C_5 h (|\mathbf{b}|_\infty + |\nabla \cdot \mathbf{b}|_\infty) \right) |u_h|_1^2 + \left(C_4 c_{\min} - \frac{1}{2} |\nabla \cdot \mathbf{b}|_\infty \right) |u_h|_0^2 \\ &\geq C |u_h|_1^2. \end{aligned}$$

This completes the proof. \square

4 Error estimate

The error estimates of scheme (2.17) in H^1 norm and L^2 norm are carried out in this section.

Let u be solution to equation (1.1) and u_h be the solution to (2.17), then we have

$$\begin{aligned} A(u - u_h, \Pi_h^* u_h) &= a(u - u_h, \Pi_h^* w_h) + b(u, \Pi_h^* w_h) \\ &\quad - b_h(u_h, \Pi_h^* w_h) + c(u - u_h, \Pi_h^* w_h) = 0. \end{aligned} \quad (4.1)$$

By coercivity, we have

$$\begin{aligned} \|\Pi_h u - u_h\|_1 &\leq \frac{1}{C} \frac{A(\Pi_h u - u_h, \Pi_h^*(\Pi_h u - u_h))}{\|\Pi_h u - u_h\|_1} \\ &\leq \frac{1}{C} \sup_{w_h \in U_h} \frac{|A(\Pi_h u - u_h, \Pi_h^* w_h)|}{\|w_h\|_1}, \end{aligned} \quad (4.2)$$

where Π_h is the bilinear interpolation operator from $H_0^1(\Omega) \cap H^2(\Omega)$ onto U_h . According to the definition $A(\cdot, \Pi_h^* \cdot)$ and (4.1), we obtain

$$\begin{aligned} &A(\Pi_h u - u_h, \Pi_h^* w_h) \\ &= a(\Pi_h u - u_h, \Pi_h^* w_h) + b_h(\Pi_h u - u_h, \Pi_h^* w_h) + c(\Pi_h u - u_h, \Pi_h^* w_h) \\ &= a(\Pi_h u - u, \Pi_h^* w_h) + b_h(\Pi_h u - u, \Pi_h^* w_h) + c(\Pi_h u - u, \Pi_h^* w_h) \\ &\quad + a(u - u_h, \Pi_h^* w_h) + b_h(u - u_h, \Pi_h^* w_h) + c(u - u_h, \Pi_h^* w_h) \\ &= a(\Pi_h u - u, \Pi_h^* w_h) + b_h(\Pi_h u - u, \Pi_h^* w_h) + (b_h(u, \Pi_h^* w_h) - b(u, \Pi_h^* w_h)) \\ &\quad + c(\Pi_h u - u, \Pi_h^* w_h). \end{aligned} \quad (4.3)$$

In order to estimate (4.3), we give four lemmas. First, for $a(\Pi_h u - u, \Pi_h^* w_h)$, we have the following estimates.

Lemma 4.1. Assume that \mathcal{T}_h is regular, and let $u \in H_0^1(\Omega) \cap H^2(\Omega)$, then there exists a constant C , such that (see [10])

$$|a(\Pi_h u - u, \Pi_h^* w_h)| \leq Ch|u|_2\|w_h\|_1, \quad \forall w_h \in U_h, \quad (4.4)$$

where constant C depends on μ_2 .

Lemma 4.2. Suppose that \mathcal{T}_h is a regular and h^2 -parallelogram partition, and let $u \in H_0^1(\Omega) \cap H^3(\Omega)$, then there exists a constant C , such that (see [14])

$$|a(\Pi_h u - u, \Pi_h^* w_h)| \leq Ch^2||u||_3\|w_h\|_1, \quad \forall w_h \in U_h, \quad (4.5)$$

where constant C depends on μ_2 .

For $(b_h(u, \Pi_h^* w_h) - b(u, \Pi_h^* w_h))$, we have the following estimate.

Lemma 4.3. Assume that \mathcal{T}_h is regular, and let $u \in H_0^1(\Omega) \cap H^2(\Omega)$, then there exists a constant C , such that

$$|b_h(u, \Pi_h^* w_h) - b(u, \Pi_h^* w_h)| \leq Ch^2|u|_2\|w_h\|_1, \quad \forall w_h \in U_h, \quad (4.6)$$

where constant C depends on \mathbf{b} .

Proof. By the definition of (2.13) and (2.19), we have

$$\begin{aligned}
& |b_h(u, \Pi_h^* w_h) - b(u, \Pi_h^* w_h)| \\
&= \left| \sum_{K_p^* \in \mathcal{T}_h^*} \int_{\partial K_p^*} (\mathbf{b} \cdot \mathbf{n})(u^{up} - u) \Pi_h^* w_h ds \right| \\
&= \left| \sum_{\sigma \in \mathcal{E}} \int_{\sigma} (\mathbf{b} \cdot \mathbf{n}) \left(u(x^{up}, y^{up}) + \mathbf{r} \cdot \nabla u(x^{up}, y^{up}) - u(x, y) \right) [\Pi_h^* w_h] ds \right|. \tag{4.7}
\end{aligned}$$

For any $\sigma \in \mathcal{E}$, without losing generality, we assume $\int_{\sigma} \mathbf{b} \cdot \mathbf{n} ds \geq 0$, as shown in Fig. 5, then we obtain

$$\begin{aligned}
& \left| \int_{\sigma} (\mathbf{b} \cdot \mathbf{n}) \left(u(x^{up}, y^{up}) + \mathbf{r} \cdot \nabla u|_K(x^{up}, y^{up}) - u(x, y) \right) [\Pi_h^* w_h] ds \right| \\
&\leq C |\mathbf{b}|_{\infty} |w_h|_{1,K} \int_0^{\frac{1}{2}} \left| \left(\hat{u}(0, \eta) + \frac{1}{2} \frac{\partial \hat{u}(0, \eta)}{\partial \xi} - \hat{u}\left(\frac{1}{2}, \eta\right) \right) \left(\left| \frac{\partial y}{\partial \eta} \right| + \left| \frac{\partial x}{\partial \eta} \right| \right) \right| d\eta \\
&\leq Ch |\mathbf{b}|_{\infty} |w_h|_{1,K} \int_0^{\frac{1}{2}} \left| \left(\hat{u}(0, \eta) + \frac{1}{2} \frac{\partial \hat{u}(0, \eta)}{\partial \xi} - \hat{u}\left(\frac{1}{2}, \eta\right) \right) \right| d\eta, \tag{4.8}
\end{aligned}$$

where $\hat{u} = u \circ F_K$, and here we use $\left| \frac{\partial y}{\partial \eta} \right| \leq Ch$, $\left| \frac{\partial x}{\partial \eta} \right| \leq Ch$. According to the Taylor expansion with integral remainder and Cauchy-Schwarz inequality, we have

$$\begin{aligned}
& \int_0^{\frac{1}{2}} \left| \left(\hat{u}(0, \eta) + \frac{1}{2} \frac{\partial \hat{u}(0, \eta)}{\partial \xi} - \hat{u}\left(\frac{1}{2}, \eta\right) \right) \right| d\eta \\
&\leq \int_0^{\frac{1}{2}} \int_0^{\frac{1}{2}} \left| \frac{1}{4} \frac{\partial^2 \hat{u}}{\partial \xi^2} \right| d\xi d\eta \leq C \left(\int_0^1 \int_0^1 \left| \frac{\partial^2 \hat{u}}{\partial \xi^2} \right|^2 d\xi d\eta \right)^{\frac{1}{2}} \leq C |\hat{u}|_{2, \hat{K}}. \tag{4.9}
\end{aligned}$$

Then, based on [43], there holds

$$|\hat{u}|_{2, \hat{K}} \leq Ch |u|_{2,K}. \tag{4.10}$$

Finally, combining (4.7)-(4.10) and using Cauchy-Schwarz inequality, we get

$$|b_h(u, \Pi_h^* w_h) - b(u, \Pi_h^* w_h)| \leq Ch^2 \sum_{\sigma \in \mathcal{E}} |w_h|_{1,K} |u|_{2,K} \leq Ch^2 |u|_2 \|w_h\|_1. \tag{4.11}$$

This completes the proof. \square

For the last part in (4.3), the following estimate holds.

Lemma 4.4. Suppose that \mathcal{T}_h is quasi-uniform, and let $u \in H_0^1(\Omega) \cap H^2(\Omega)$, then there exists a constant C , such that

$$|b_h(u - \Pi_h u, \Pi_h^* w_h)| \leq Ch^2 |u|_2 \|w_h\|_1, \quad \forall w_h \in U_h, \quad (4.12)$$

where constant C depends on \mathbf{b} .

Proof. In accordance with the definition of (2.13), we have

$$\begin{aligned} & |b_h(u - \Pi_h u, \Pi_h^* w_h)| \\ &= \left| \sum_{K_P^* \in \mathcal{T}_h^*} \int_{\partial K_P^*} (\mathbf{b} \cdot \mathbf{n})(u^{up} - (\Pi_h u)^{up}) \Pi_h^* w_h ds \right| \\ &= \left| \sum_{\sigma \in \mathcal{E}} \int_{\sigma} (\mathbf{b} \cdot \mathbf{n}) \left(u(x^{up}, y^{up}) + \mathbf{r} \cdot \nabla u(x^{up}, y^{up}) \right. \right. \\ &\quad \left. \left. - (\Pi_h u)(x^{up}, y^{up}) - \mathbf{r} \cdot \bar{\nabla}(\Pi_h u)(x^{up}, y^{up}) \right) [\Pi_h^* w_h] ds \right|. \end{aligned} \quad (4.13)$$

For any $\sigma \in \mathcal{E}$, without losing generality, we assume $\int_{\sigma} \mathbf{b} \cdot \mathbf{n} ds \geq 0$, then we obtain

$$\begin{aligned} & \left| \int_{\sigma} (\mathbf{b} \cdot \mathbf{n}) \left(u(x^{up}, y^{up}) + \mathbf{r} \cdot \nabla u(x^{up}, y^{up}) \right. \right. \\ &\quad \left. \left. - (\Pi_h u)(x^{up}, y^{up}) - \mathbf{r} \cdot \bar{\nabla}(\Pi_h u)(x^{up}, y^{up}) \right) [\Pi_h^* w_h] ds \right| \\ &\leq C |\mathbf{b}|_{\infty} |w_h|_{1,K} \left(\int_{\sigma} \left| u(x^{up}, y^{up}) - (\Pi_h u)(x^{up}, y^{up}) \right| ds \right. \\ &\quad + \frac{h}{2} \int_{\sigma} \left| \nabla u|_K(x^{up}, y^{up}) - \nabla(\Pi_h u)|_K(x^{up}, y^{up}) \right| ds \\ &\quad \left. + \frac{h}{2} \int_{\sigma} \left| \nabla u|_{K^{up}}(x^{up}, y^{up}) - \nabla(\Pi_h u)|_{K^{up}}(x^{up}, y^{up}) \right| ds \right). \end{aligned} \quad (4.14)$$

Firstly, for the integral $\int_{\sigma} |u(x^{up}, y^{up}) - (\Pi_h u)(x^{up}, y^{up})| ds$, by taking $g_1(x, y) = u(x, y) - (\Pi_h u)(x, y)$, we have

$$\int_{\sigma} |g_1| ds \leq C \int_0^{\frac{1}{2}} \left| \hat{g}_1(0, \eta) \left(\left| \frac{\partial y}{\partial \eta} \right| + \left| \frac{\partial x}{\partial \eta} \right| \right) \right| d\eta \leq Ch \int_0^{\frac{1}{2}} \left| \hat{g}_1(0, \eta) \right| d\eta. \quad (4.15)$$

Utilizing Cauchy-Schwarz inequality, we get

$$\begin{aligned}
\int_0^{\frac{1}{2}} |\hat{g}_1(0, \eta)| d\eta &= \int_0^{\frac{1}{2}} \left| \int_0^1 \frac{\partial((\xi-1)\hat{g}_1(\xi, \eta))}{\partial\xi} d\xi \right| d\eta \\
&\leq \int_0^1 \int_0^1 |\hat{g}_1(\xi, \eta)| d\xi d\eta + \int_0^1 \int_0^1 \left| (\xi-1) \frac{\partial \hat{g}_1(\xi, \eta)}{\partial\xi} \right| d\xi d\eta \\
&\leq \int_0^1 \int_0^1 |\hat{g}_1(\xi, \eta)| d\xi d\eta + \int_0^1 \int_0^1 \left| \frac{\partial \hat{g}_1(\xi, \eta)}{\partial\xi} \right| d\xi d\eta \\
&\leq C|\hat{g}_1|_{0,\hat{K}} + C|\hat{g}_1|_{1,\hat{K}}.
\end{aligned} \tag{4.16}$$

Then, based on [43] and estimate of interpolation error, there holds

$$|\hat{g}_1|_{0,\hat{K}} \leq Ch^{-1}|u - \Pi_h u|_{0,K} \leq Ch|u|_{2,K}, \tag{4.17}$$

$$|\hat{g}_1|_{1,\hat{K}} \leq C|u - \Pi_h u|_{1,K} \leq Ch|u|_{2,K}. \tag{4.18}$$

Then, we get

$$\int_\sigma \left| u(x^{up}, y^{up}) - (\Pi_h u)(x^{up}, y^{up}) \right| ds \leq Ch^2|u|_{2,K}. \tag{4.19}$$

Next, for the integral $\int_\sigma |\nabla u|_K(x^{up}, y^{up}) - \nabla(\Pi_h u)|_K(x^{up}, y^{up})| ds$, we take $g_2(x, y) = |\nabla u|_K(x, y) - \nabla(\Pi_h u)|_K(x, y)|$, similar to (4.15) and (4.16), we have

$$\int_\sigma |g_2| ds \leq Ch|\hat{g}_2|_{0,\hat{K}} + Ch|\hat{g}_2|_{1,\hat{K}}. \tag{4.20}$$

Based on [43] and estimate of interpolation error, there holds

$$|\hat{g}_2|_{0,\hat{K}} \leq Ch^{-1}|g_2|_{0,K} \leq Ch^{-1}|u - \Pi_h u|_{1,K} \leq C|u|_{2,K}, \tag{4.21}$$

$$|\hat{g}_2|_{1,\hat{K}} \leq C|g_2|_{1,K} \leq C|u - \Pi_h u|_{2,K} \leq C|u|_{2,K}. \tag{4.22}$$

Then, we get

$$\int_\sigma \left| \nabla u|_K(x^{up}, y^{up}) - \nabla(\Pi_h u)|_K(x^{up}, y^{up}) \right| ds \leq Ch|u|_{2,K}. \tag{4.23}$$

For the integral $\int_\sigma |\nabla u|_{K^{up}}(x^{up}, y^{up}) - \nabla(\Pi_h u)|_{K^{up}}(x^{up}, y^{up})| ds$, we take $g_3(x, y) = |\nabla u|_{K^{up}}(x, y) - \nabla(\Pi_h u)|_{K^{up}}(x, y)|$, similar to (4.15), we have

$$\int_\sigma |g_3| ds \leq Ch \int_0^{\frac{1}{2}} |\hat{g}_3(1, \eta)| d\eta. \tag{4.24}$$

By using Cauchy-Schwarz inequality, similar to (4.16), we have

$$\begin{aligned}
\int_0^{\frac{1}{2}} |\hat{g}_3(1, \eta)| d\eta &= \int_0^{\frac{1}{2}} \left| \int_0^1 \frac{\partial(\xi \hat{g}_3(\xi, \eta))}{\partial \xi} d\xi \right| d\eta \\
&\leq \int_0^1 \int_0^1 |\hat{g}_3(\xi, \eta)| d\xi d\eta + \int_0^1 \int_0^1 \left| \frac{\partial \hat{g}_3(\xi, \eta)}{\partial \xi} \right| d\xi d\eta \\
&\leq C|\hat{g}_3|_{0, \hat{K}^{up}} + C|\hat{g}_3|_{1, \hat{K}^{up}}.
\end{aligned} \tag{4.25}$$

Based on [43] and estimate of interpolation error, there holds

$$|\hat{g}_3|_{0, \hat{K}^{up}} \leq Ch^{-1}|g_3|_{0, \hat{K}^{up}} \leq Ch^{-1}|u - \Pi_h u|_{1, K^{up}} \leq C|u|_{2, K^{up}}, \tag{4.26}$$

$$|\hat{g}_3|_{1, \hat{K}^{up}} \leq C|g_3|_{1, \hat{K}^{up}} \leq C|u - \Pi_h u|_{2, K^{up}} \leq C|u|_{2, K^{up}}. \tag{4.27}$$

Hence, we have

$$\int_\sigma \left| \nabla u|_{K^{up}}(x^{up}, y^{up}) - \nabla(\Pi_h u)|_{K^{up}}(x^{up}, y^{up}) \right| ds \leq Ch|u|_{2, K^{up}}. \tag{4.28}$$

Combine (4.13)-(4.14), (4.19), (4.23) and (4.28) and using Cauchy-Schwarz inequality, then we get

$$\begin{aligned}
|b_h(u - \Pi_h u, \Pi_h^* w_h)| &\leq Ch^2 \sum_{\sigma \in \mathcal{E}} |w_h|_{1, K} (|u|_{2, K} + |u|_{2, K^{up}}) \\
&\leq Ch^2|u|_2 \|w_h\|_1.
\end{aligned}$$

This completes the proof. \square

For $c(\Pi_h u - u, \Pi_h^* w_h)$, we have the following estimate. Let $c_{\max} = \max_{(x, y) \in \Omega} (|c(x, y)|)$.

Lemma 4.5. Assume that \mathcal{T}_h is regular, and let $u \in H_0^1(\Omega) \cap H^2(\Omega)$, then there exists a constant C , such that

$$|c(\Pi_h u - u, \Pi_h^* w_h)| \leq Ch^2|u|_2 \|w_h\|_1, \quad \forall w_h \in U_h, \tag{4.29}$$

where constant C depends on c_{\max} .

Proof. According to the estimate of interpolation error, we have

$$\begin{aligned}
|c(\Pi_h u - u, \Pi_h^* w_h)| &\leq C\|\Pi_h u - u\|_0 \|w_h\|_0 \\
&\leq Ch^2|u|_2 \|w_h\|_0 \\
&\leq Ch^2|u|_2 \|w_h\|_1.
\end{aligned}$$

This completes the proof. \square

On the basis of Lemmas 4.1, 4.3, 4.4 and 4.5, we can obtain the following H^1 norm error estimate.

Theorem 4.1. Suppose that \mathcal{T}_h is a quasi-uniform and $h^{1+\gamma}$ -parallelogram partition ($0 < \gamma \leq 1$), let $u \in H_0^1(\Omega) \cap H^2(\Omega)$ and $u_h \in U_h$ be the solution to (1.1) and (2.17), then there exists a constant C , such that

$$\|u - u_h\|_1 \leq Ch|u|_2, \quad (4.30)$$

where constant C depends on γ , $\mu_i (i=1,2)$, \mathbf{b} and c_{\max} .

Proof. Based on (4.2)-(4.3), Lemmas 4.1, 4.3, 4.4 and 4.5, we obtain

$$\|\Pi_h u - u_h\|_1 \leq \frac{1}{C} \sup_{w_h \in U_h} \frac{|A(\Pi_h u - u_h, \Pi_h^* w_h)|}{\|w_h\|_1} \leq Ch|u|_2. \quad (4.31)$$

Then according to estimate of interpolation error, we get

$$\begin{aligned} \|u - u_h\|_1 &= \|u - \Pi_h u + \Pi_h u - u_h\|_1 \\ &\leq \|u - \Pi_h u\|_1 + \|\Pi_h u - u_h\|_1 \\ &\leq Ch|u|_2. \end{aligned} \quad (4.32)$$

This completes the proof. \square

With the help of Lemmas 4.2, 4.3, 4.4 and 4.5, we have the following superconvergence result.

Corollary 4.1. Assume that \mathcal{T}_h is a quasi-uniform and h^2 -parallelogram partition, let $u \in H_0^1(\Omega) \cap H^3(\Omega)$ and $u_h \in U_h$ be the solution to (1.1) and (2.17), then there exists a constant C , such that

$$\|u_h - \Pi_h u\|_1 \leq Ch^2\|u\|_3, \quad (4.33)$$

where constant C depends on $\mu_i (i=1,2)$, \mathbf{b} and c_{\max} .

Finally, with the help of superconvergence result, we can directly obtain the L^2 norm error estimate.

Theorem 4.2. Suppose that \mathcal{T}_h is a quasi-uniform and h^2 -parallelogram partition, let $u \in H_0^1(\Omega) \cap H^3(\Omega)$ and $u_h \in U_h$ be the solution to (1.1) and (2.17), then there exists a constant C , such that

$$\|u - u_h\|_0 \leq Ch^2\|u\|_3, \quad (4.34)$$

where constant C depends on $\mu_i (i=1,2)$, \mathbf{b} and c_{\max} .

Proof. Utilizing triangular inequality and Corollary 4.1, there holds that

$$\begin{aligned} \|u - u_h\|_0 &= \|u - \Pi_h u + \Pi_h u - u_h\|_0 \\ &\leq \|u - \Pi_h u\|_0 + \|\Pi_h u - u_h\|_1 \\ &\leq Ch^2 \|u\|_3. \end{aligned} \quad (4.35)$$

This completes the proof. \square

Remark 4.1. For theoretical analysis of FVEM, the meshes are usually required to satisfy some conditions, such as $h^{1+\gamma}$ -parallelogram condition [10, 14, 18, 20]. For bilinear element FVEM, under h^2 -parallelogram condition, stability analysis and H^1 error estimate are established in [10], the optimal L^2 error estimate is established in [14]. For bi- k element FVEM ($k \geq 1$), stability analysis is established under $h^{1+\gamma}$ -parallelogram condition ($\gamma > 0$) in [18], and the optimal L^2 error estimate is proved under $h^{1+\gamma}$ -parallelogram condition ($\gamma \geq \frac{k+1}{2k}$) in [20]. We would like to point out that, for bilinear element FVEM, the condition in paper [20] is the same as the condition in paper [14]. Until now, the h^2 -parallelogram condition is still needed for optimal L^2 error estimate of bilinear element FVEM. However, a large number of numerical experiments show that these conditions are sufficient for theoretical analysis, but are not necessary for numerical implementation, see [14, 18, 20, 45]. We verify that $h^{1+\gamma}$ -parallelogram condition is not necessary by numerical experiment, see Example 5.5.

5 Numerical examples

In this section, we present several numerical examples to demonstrate the theoretical results proved in previous sections. For the discrete solution u_h and the exact solution u , we calculate the errors by following continuous H^1 semi-norm, L^2 norm and discrete L^2 norm

$$\|u - u_h\|_1 = \left(\sum_{K \in \mathcal{T}_h} \int_K \left[\left(\frac{\partial u}{\partial x} - \frac{\partial u_h}{\partial x} \right)^2 + \left(\frac{\partial u}{\partial y} - \frac{\partial u_h}{\partial y} \right)^2 \right] dx dy \right)^{\frac{1}{2}}, \quad (5.1)$$

$$\|u - u_h\|_0 = \left(\sum_{K \in \mathcal{T}_h} \int_K (u - u_h)^2 dx dy \right)^{\frac{1}{2}}, \quad (5.2)$$

$$\|u - u_h\|_{0,h} = \left(\sum_{K_P^* \in \mathcal{T}_h^*} (u(P) - u_P)^2 |K_P^*| \right)^{\frac{1}{2}}. \quad (5.3)$$

The rate of convergence is obtained by the following formula,

$$\text{Rate} = \log \left(\frac{e(h_1)}{e(h_2)} \right) / \log \left(\frac{h_1}{h_2} \right), \quad (5.4)$$

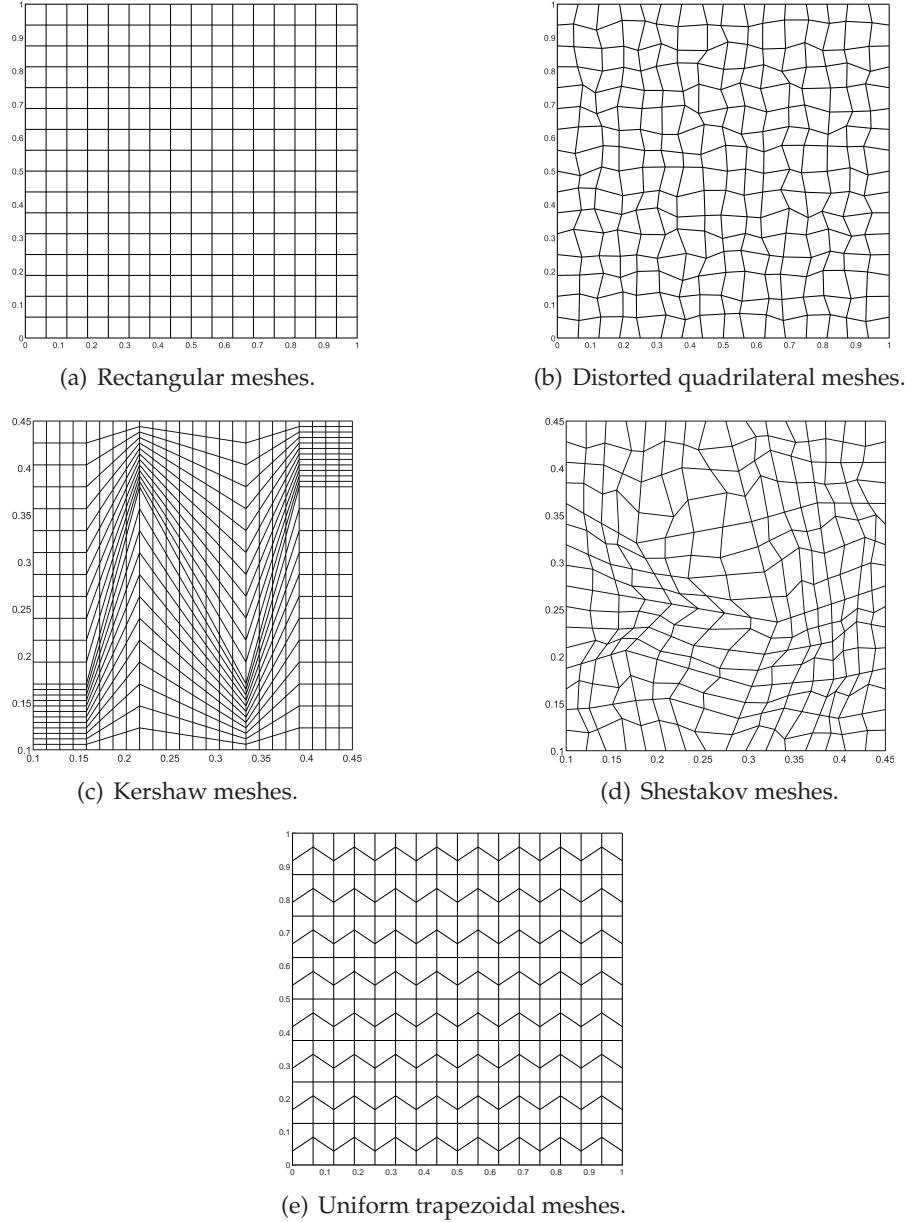


Figure 6: Five types of meshes.

where h_1, h_2 are the mesh sizes of the two successive meshes, $e(h_1)$ and $e(h_2)$ denote the corresponding discrete errors. In the numerical tests, we use rectangular meshes, distorted(perturbed) quadrilateral meshes, Kershaw meshes, Shestakov meshes or uniform trapezoidal meshes, see Fig. 6.

5.1 Scalar diffusion problem

In this part, we compare the scheme (NUFVM) proposed in this paper with the standard upwind finite volume element method (SUFVM) [29], optimal weighted upwind finite volume element method (OWUFVM) [42], and complete flux scheme(CFS) [38]. Considering SUFVM, OWUFVM and CFS can only deal with scalar diffusion on rectangular meshes, so we calculate Examples 5.1 and 5.2 on rectangular meshes. According to the definition of CFS, we use discrete L^2 norm (5.3) to calculate errors in this part.

Example 5.1. We consider Eq. (1.1) with Dirichlet boundary condition on domain $\Omega = [0,1]^2$. We take the scalar diffusion coefficient $\kappa(x,y) = D\mathbf{I}_2$, where D is constant and \mathbf{I}_2 is the identity matrix. Take the constant convection velocity $\mathbf{b} = (2,1)^T$. The exact solution is chosen to be

$$u(x,y) = 1 - e^{2x+y-3/D} + e^{x+y}. \quad (5.5)$$

The source term f and the boundary value are set according to the exact solution u .

Example 5.2. We discuss the equation (1.1) with Dirichlet boundary condition on $\Omega = [0,1]^2$. We take the scalar diffusion coefficient $\kappa(x,y) = D\mathbf{I}_2$, where D is constant and \mathbf{I}_2 is the identity matrix. The variable convection velocity is taken as $\mathbf{b} = (2-x^2y, 1+xy^2)^T$. The exact solution is

$$u(x,y) = 1 - e^{2x+y-3/D} + e^{x+y}. \quad (5.6)$$

The source term f and the boundary value are given by the exact solution u .

The numerical results of NUFVM, SUFVM, OWUFVM and CFS are shown in Tables 1-4. For the convergence rate in H^1 semi-norm, when the convection is strongly dominant, SUFVM is $\mathcal{O}(h^{\frac{1}{2}})$. However, OWUFVM and NUFVM are $\mathcal{O}(h)$. Due to CFS does not have the definition in H^1 norm, so we do not list the convergence rate of CFS in H^1 norm. For the convergence rate in L^2 norm, SUFVM is $\mathcal{O}(h)$, and OWUFVM, CFS and NUFVM are $\mathcal{O}(h^2)$. In addition, for L^2 norm error, the errors of OWUFVM are smallest, and the errors of CFS and NUFVM are close. For H^1 semi-norm error, the errors of OWUFVM and NUFVM are close. Moreover, CFS and OWUFVM are not defined on general quadrilateral meshes and can not deal with anisotropic diffusion.

5.2 Anisotropic diffusion problem

In this part, we compare NUFVM with the generalised complete flux scheme (GCFS) in [39] on rectangular meshes. We use discrete L^2 norm (5.3) to calculate errors in this part.

Table 1: Convergence rate of H^1 semi-norm for Example 5.1 on rectangular meshes.

D	h	SUFVM		OWUFVM		NUFVM	
		$ u - u_h _1$	Rate	$ u - u_h _1$	Rate	$ u - u_h _1$	Rate
1	$1/2^5$	3.6220×10^{-2}	-	3.1375×10^{-2}	-	3.1375×10^{-2}	-
	$1/2^6$	1.8170×10^{-2}	0.9952	1.5687×10^{-2}	1.0000	1.5687×10^{-2}	1.0000
	$1/2^7$	9.1001×10^{-3}	0.9976	7.8435×10^{-3}	1.0000	7.8435×10^{-3}	1.0000
	$1/2^8$	4.5537×10^{-3}	0.9988	3.9218×10^{-3}	1.0000	3.9218×10^{-3}	1.0000
	$1/2^9$	2.2778×10^{-3}	0.9994	1.9609×10^{-3}	1.0000	1.9609×10^{-3}	1.0000
10^{-6}	$1/2^5$	3.9181×10^{-1}	-	4.0807×10^{-2}	-	4.1803×10^{-2}	-
	$1/2^6$	2.8386×10^{-1}	0.4650	2.0391×10^{-2}	1.0009	2.0653×10^{-2}	1.0173
	$1/2^7$	2.0315×10^{-1}	0.4827	1.0192×10^{-2}	1.0005	1.0259×10^{-2}	1.0094
	$1/2^8$	1.4450×10^{-1}	0.4915	5.0952×10^{-3}	1.0002	5.1123×10^{-3}	1.0049
	$1/2^9$	1.0246×10^{-1}	0.4959	2.5474×10^{-3}	1.0001	2.5517×10^{-3}	1.0025
10^{-8}	$1/2^5$	3.9182×10^{-1}	-	4.0807×10^{-2}	-	4.1803×10^{-2}	-
	$1/2^6$	2.8387×10^{-1}	0.4649	2.0391×10^{-2}	1.0009	2.0653×10^{-2}	1.0173
	$1/2^7$	2.0317×10^{-1}	0.4826	1.0192×10^{-2}	1.0005	1.0259×10^{-2}	1.0094
	$1/2^8$	1.4453×10^{-1}	0.4913	5.0952×10^{-3}	1.0002	5.1123×10^{-3}	1.0049
	$1/2^9$	1.0250×10^{-1}	0.4957	2.5474×10^{-3}	1.0001	2.5517×10^{-3}	1.0025

Table 2: Convergence rate of L^2 norm for Example 5.1 on rectangular meshes.

D	h	SUFVM		OWUFVM		CFS		NUFVM	
		$\ u - u_h\ _{0,h}$	Rate						
1	$1/2^5$	4.15×10^{-3}	-	6.86×10^{-6}	-	8.88×10^{-6}	-	2.32×10^{-5}	-
	$1/2^6$	2.01×10^{-3}	1.04	1.71×10^{-6}	2.00	2.26×10^{-6}	1.98	4.66×10^{-6}	2.32
	$1/2^7$	9.90×10^{-4}	1.02	4.29×10^{-7}	2.00	5.69×10^{-7}	1.99	1.02×10^{-6}	2.19
	$1/2^8$	4.91×10^{-4}	1.01	1.07×10^{-7}	2.00	1.43×10^{-7}	1.99	2.39×10^{-7}	2.10
	$1/2^9$	2.45×10^{-4}	1.01	2.68×10^{-8}	2.00	3.58×10^{-8}	2.00	5.76×10^{-8}	2.05
10^{-6}	$1/2^5$	2.81×10^{-2}	-	1.47×10^{-4}	-	2.93×10^{-4}	-	6.53×10^{-4}	-
	$1/2^6$	1.44×10^{-2}	0.96	3.76×10^{-5}	1.97	7.51×10^{-5}	1.97	1.65×10^{-4}	1.98
	$1/2^7$	7.29×10^{-3}	0.98	9.51×10^{-6}	1.98	1.90×10^{-5}	1.98	4.15×10^{-5}	1.99
	$1/2^8$	3.67×10^{-3}	0.99	2.39×10^{-6}	1.99	4.78×10^{-6}	1.99	1.04×10^{-5}	2.00
	$1/2^9$	1.84×10^{-3}	1.00	5.99×10^{-7}	2.00	1.20×10^{-6}	2.00	2.60×10^{-6}	2.00
10^{-8}	$1/2^5$	2.81×10^{-2}	-	1.47×10^{-4}	-	2.93×10^{-4}	-	6.53×10^{-4}	-
	$1/2^6$	1.44×10^{-2}	0.96	3.76×10^{-5}	1.97	7.51×10^{-5}	1.97	1.65×10^{-4}	1.98
	$1/2^7$	7.29×10^{-3}	0.98	9.51×10^{-6}	1.98	1.90×10^{-5}	1.98	4.15×10^{-5}	1.99
	$1/2^8$	3.67×10^{-3}	0.99	2.39×10^{-6}	1.99	4.78×10^{-6}	1.99	1.04×10^{-5}	2.00
	$1/2^9$	1.84×10^{-3}	1.00	5.99×10^{-7}	2.00	1.20×10^{-6}	2.00	2.61×10^{-6}	2.00

Table 3: Convergence rate of H^1 semi-norm for Example 5.2 on rectangular meshes.

D	h	SUFVM		OWUFVM		NUFVM	
		$ u - u_h _1$	Rate	$ u - u_h _1$	Rate	$ u - u_h _1$	Rate
1	$1/2^5$	3.3455×10^{-1}	-	3.1374×10^{-2}	-	3.1375×10^{-2}	-
	$1/2^6$	2.1254×10^{-1}	0.9944	1.5687×10^{-2}	1.0000	1.5687×10^{-2}	1.0000
	$1/2^7$	1.2579×10^{-1}	0.9972	7.8435×10^{-3}	1.0000	7.8435×10^{-3}	1.0000
	$1/2^8$	7.0082×10^{-2}	0.9986	3.9218×10^{-3}	1.0000	3.9218×10^{-3}	1.0000
	$1/2^9$	3.7345×10^{-2}	0.9993	1.9609×10^{-3}	1.0000	1.9609×10^{-3}	1.0000
10^{-6}	$1/2^5$	4.0557×10^{-1}	-	4.0811×10^{-2}	-	4.1739×10^{-2}	-
	$1/2^6$	2.9479×10^{-1}	0.4603	2.0392×10^{-2}	1.0010	2.0636×10^{-2}	1.0163
	$1/2^7$	2.1132×10^{-1}	0.4803	1.0192×10^{-2}	1.0005	1.0255×10^{-2}	1.0088
	$1/2^8$	1.5044×10^{-1}	0.4903	5.0953×10^{-3}	1.0003	5.1111×10^{-3}	1.0046
	$1/2^9$	1.0672×10^{-1}	0.4954	2.5474×10^{-3}	1.0001	2.5514×10^{-3}	1.0023
10^{-8}	$1/2^5$	4.0558×10^{-1}	-	4.0811×10^{-2}	-	4.1739×10^{-2}	-
	$1/2^6$	2.9481×10^{-1}	0.4602	2.0392×10^{-2}	1.0010	2.0636×10^{-2}	1.0163
	$1/2^7$	2.1134×10^{-1}	0.4802	1.0192×10^{-2}	1.0005	1.0255×10^{-2}	1.0088
	$1/2^8$	1.5046×10^{-1}	0.4902	5.0953×10^{-3}	1.0003	5.1111×10^{-3}	1.0046
	$1/2^9$	1.0676×10^{-1}	0.4951	2.5474×10^{-3}	1.0001	2.5514×10^{-3}	1.0023

Table 4: Convergence rate of L^2 norm for Example 5.2 on rectangular meshes.

D	h	SUFVM		OWUFVM		CFS		NUFVM	
		$\ u - u_h\ _{0,h}$	Rate						
1	$1/2^5$	4.34×10^{-3}	-	4.98×10^{-6}	-	2.00×10^{-5}	-	2.82×10^{-5}	-
	$1/2^6$	2.11×10^{-3}	1.04	1.25×10^{-6}	2.00	5.07×10^{-6}	1.98	6.00×10^{-6}	2.23
	$1/2^7$	1.04×10^{-3}	1.02	3.11×10^{-7}	2.00	1.28×10^{-6}	1.99	1.37×10^{-6}	2.13
	$1/2^8$	5.17×10^{-4}	1.01	7.78×10^{-8}	2.00	3.21×10^{-7}	1.99	3.29×10^{-7}	2.06
	$1/2^9$	2.57×10^{-4}	1.00	1.95×10^{-8}	2.00	8.03×10^{-8}	2.00	8.03×10^{-8}	2.03
10^{-6}	$1/2^5$	2.88×10^{-2}	-	1.51×10^{-4}	-	3.70×10^{-4}	-	6.41×10^{-4}	-
	$1/2^6$	1.48×10^{-2}	0.96	3.87×10^{-5}	1.96	9.48×10^{-5}	1.96	1.61×10^{-4}	1.99
	$1/2^7$	7.50×10^{-3}	0.98	9.79×10^{-6}	1.98	2.40×10^{-5}	1.98	4.07×10^{-5}	1.99
	$1/2^8$	3.78×10^{-3}	0.99	2.46×10^{-6}	1.99	6.03×10^{-6}	1.99	1.02×10^{-5}	2.00
	$1/2^9$	1.90×10^{-3}	1.00	6.18×10^{-7}	2.00	1.51×10^{-6}	2.00	2.55×10^{-6}	2.00
10^{-8}	$1/2^5$	2.88×10^{-2}	-	1.51×10^{-4}	-	3.70×10^{-4}	-	6.41×10^{-4}	-
	$1/2^6$	1.48×10^{-2}	0.96	3.87×10^{-5}	1.96	9.48×10^{-5}	1.96	1.62×10^{-4}	1.99
	$1/2^7$	7.51×10^{-3}	0.98	9.79×10^{-6}	1.98	2.40×10^{-5}	1.98	4.07×10^{-5}	1.99
	$1/2^8$	3.78×10^{-3}	0.99	2.46×10^{-6}	1.99	6.03×10^{-6}	1.99	1.02×10^{-5}	2.00
	$1/2^9$	1.90×10^{-3}	1.00	6.18×10^{-7}	2.00	1.51×10^{-6}	2.00	2.55×10^{-6}	2.00

Example 5.3. In this part, we consider the convection-diffusion problem with anisotropic diffusion tensor in paper [39]. Set the domain $\Omega = [0,1]^2$. Take the variable convection velocity $\mathbf{b} = (1,2)^T$. The exact solution is

$$u(x,y) = \sin(\pi x) \sin(\pi y). \quad (5.7)$$

We take the rotating anisotropic diffusion tensor as follows:

$$\kappa(x,y) = \frac{1}{2}D \begin{pmatrix} 1+10^{-8} & 1-10^{-8} \\ 1-10^{-8} & 1+10^{-8} \end{pmatrix},$$

where D is a constant. The eigenvalues of diffusion tensor are given by $\lambda_1 = 10^{-8}D$ and $\lambda_2 = D$. So the diffusion tensor is strong anisotropy. The source term f and the Dirichlet boundary value are set according to the exact solution.

As shown in Table 5, two schemes both have second-order accuracy in L^2 norm, but the errors of NUFVM are smaller. We also list the numerical results for NUFVM on distorted quadrilateral meshes. As shown in Table 6, we can see that the convergence rate of H^1 semi-norm is $\mathcal{O}(h)$ and L^2 norm is $\mathcal{O}(h^2)$.

Table 5: Convergence rate of L^2 norm in for Example 5.3 on rectangular meshes.

D	h	GCFS		NUFVM	
		$\ u - u_h\ _{0,h}$	Rate	$\ u - u_h\ _{0,h}$	Rate
1	$1/2^4$	2.3603×10^{-3}	-	1.5189×10^{-3}	-
	$1/2^5$	5.8254×10^{-4}	2.0186	4.1770×10^{-4}	1.8625
	$1/2^6$	1.4418×10^{-4}	2.0144	1.0940×10^{-4}	1.9329
	$1/2^7$	3.5834×10^{-5}	2.0085	2.7988×10^{-5}	1.9667
	$1/2^8$	8.9301×10^{-6}	2.0046	7.0781×10^{-6}	1.9834
	$1/2^9$	2.2289×10^{-6}	2.0024	1.7797×10^{-6}	1.9917
10^{-6}	$1/2^4$	5.0946×10^{-3}	-	1.7749×10^{-3}	-
	$1/2^5$	1.2706×10^{-3}	2.0034	3.1747×10^{-4}	2.4830
	$1/2^6$	3.1727×10^{-4}	2.0017	6.4127×10^{-5}	2.3076
	$1/2^7$	7.9107×10^{-5}	2.0038	1.4229×10^{-5}	2.1720
	$1/2^8$	1.9585×10^{-5}	2.0140	3.3427×10^{-6}	2.0898
	$1/2^9$	4.7408×10^{-6}	2.0466	8.0969×10^{-7}	2.0456
10^{-8}	$1/2^4$	5.0949×10^{-3}	-	1.7749×10^{-3}	-
	$1/2^5$	1.2709×10^{-3}	2.0032	3.1747×10^{-4}	2.4830
	$1/2^6$	3.1754×10^{-4}	2.0008	6.4127×10^{-5}	2.3076
	$1/2^7$	7.9373×10^{-5}	2.0002	1.4229×10^{-5}	2.1720
	$1/2^8$	1.9841×10^{-5}	2.0002	3.3427×10^{-6}	2.0898
	$1/2^9$	4.9581×10^{-6}	2.0006	8.0969×10^{-7}	2.0456

Table 6: Convergence rate of NUFVM for Example 5.3 on distorted quadrilateral meshes.

D	h	$ u - u_h _1$	Rate	$\ u - u_h\ _0$	Rate
1	$1/2^5$	7.7600×10^{-2}	-	8.5187×10^{-4}	-
	$1/2^6$	3.9142×10^{-2}	0.9873	2.0964×10^{-4}	2.0227
	$1/2^7$	1.9710×10^{-2}	0.9898	5.5785×10^{-5}	1.9100
	$1/2^8$	9.8401×10^{-3}	1.0022	1.4344×10^{-5}	1.9595
	$1/2^9$	4.9390×10^{-3}	0.9945	3.7499×10^{-6}	1.9355
10^{-6}	$1/2^5$	7.7661×10^{-2}	-	1.2550×10^{-3}	-
	$1/2^6$	3.8367×10^{-2}	1.0173	3.0752×10^{-4}	2.0290
	$1/2^7$	1.9281×10^{-2}	0.9927	7.5650×10^{-5}	2.0233
	$1/2^8$	9.6735×10^{-3}	0.9951	1.8858×10^{-5}	2.0042
	$1/2^9$	4.8305×10^{-3}	1.0019	4.6850×10^{-6}	2.0090
10^{-8}	$1/2^5$	7.5781×10^{-2}	-	1.2201×10^{-3}	-
	$1/2^6$	3.8348×10^{-2}	0.9827	2.9947×10^{-4}	2.0265
	$1/2^7$	1.9268×10^{-2}	0.9929	7.3184×10^{-5}	2.0328
	$1/2^8$	9.6744×10^{-3}	0.9940	1.8338×10^{-5}	1.9967
	$1/2^9$	4.8350×10^{-3}	1.0007	4.7342×10^{-6}	1.9536

Example 5.4. In this part, we consider the convection-diffusion problem with heterogeneous anisotropic diffusion tensor. The computational domain is $\Omega = [0,1]^2$. Take the variable convection velocity $\mathbf{b} = (2-x^2y, 1+xy^2)^T$. The exact solution is

$$u(x,y) = \sin(\pi x) \sin(\pi y). \quad (5.8)$$

We take the heterogeneous anisotropic diffusion tensor as follows:

$$\kappa(x,y) = \frac{D}{x^2+y^2} \begin{pmatrix} \alpha x^2 + y^2 & (\alpha-1)xy \\ (\alpha-1)xy & x^2 + \alpha y^2 \end{pmatrix},$$

where D is a constant and $\alpha = 10^{-6}$ depicts the level of anisotropy. The source term f and the Dirichlet boundary value are set according to the exact solution. From Table 7, we can see that the convergence rate of H^1 semi-norm is $\mathcal{O}(h)$ and L^2 norm is $\mathcal{O}(h^2)$.

5.3 Convection-diffusion on special meshes

Example 5.5. The computational domain is $\Omega = [0,1]^2$. Take the variable convection velocity $\mathbf{b} = (2-x^2y, 1+xy^2)^T$. The exact solution is

$$u(x,y) = \sin(\pi x) \sin(\pi y). \quad (5.9)$$

Table 7: Convergence rate for Example 5.4 on distorted quadrilateral meshes.

D	h	$ u - u_h _1$	Rate	$\ u - u_h\ _0$	Rate
1	$1/2^5$	7.6501×10^{-2}	-	7.2631×10^{-4}	-
	$1/2^6$	3.8666×10^{-2}	0.9844	1.8268×10^{-4}	1.9912
	$1/2^7$	1.9658×10^{-2}	0.9759	4.8459×10^{-5}	1.9145
	$1/2^8$	9.9086×10^{-3}	0.9884	1.2952×10^{-5}	1.9036
	$1/2^9$	4.9985×10^{-3}	0.9872	3.5734×10^{-6}	1.8577
10^{-6}	$1/2^5$	7.6184×10^{-2}	-	1.2054×10^{-3}	-
	$1/2^6$	3.8320×10^{-2}	0.9914	2.9860×10^{-4}	2.0132
	$1/2^7$	1.9268×10^{-2}	0.9919	7.3588×10^{-5}	2.0207
	$1/2^8$	9.6742×10^{-3}	0.9940	1.8893×10^{-5}	1.9616
	$1/2^9$	4.8393×10^{-3}	0.9993	4.7386×10^{-6}	1.9953
10^{-8}	$1/2^5$	7.6481×10^{-2}	-	1.1904×10^{-3}	-
	$1/2^6$	3.8326×10^{-2}	0.9968	2.9496×10^{-4}	2.0129
	$1/2^7$	1.9286×10^{-2}	0.9907	7.8321×10^{-5}	1.9131
	$1/2^8$	9.7001×10^{-3}	0.9915	1.9158×10^{-5}	2.0314
	$1/2^9$	4.8400×10^{-3}	1.0030	4.6320×10^{-6}	2.0483

We take the variable diffusion tensor as follows:

$$\kappa(x, y) = D \begin{pmatrix} 1+2x^2+y^2 & 0 \\ 0 & 1+x^2+2y^2 \end{pmatrix},$$

where D is a constant. The source term f and the Dirichlet boundary value are set according to the exact solution. Obviously, for the fixed constant D , the eigenvalues of diffusion tensor have following relationship. When $x > y$ ($x < y$), the eigenvalue in x -direction is greater (less) than that in y -direction. The eigenvalues with the largest difference are given by $\lambda_1 = 2D$ and $\lambda_2 = 3D$. The eigenvalues with the smallest difference are $\lambda_1 = \lambda_2$ on line $x = y$. So the diffusion tensor is mild anisotropy.

In Fig. 6, we demonstrate some meshes, it is easy to verify that Kershaw meshes satisfy the h^2 -parallelogram condition, and uniform trapezoidal meshes do not satisfy the $h^{1+\gamma}$ -parallelogram condition. Distorted quadrilateral meshes and Shestakov meshes are random disturbed meshes, which usually do not satisfy $h^{1+\gamma}$ -parallelogram condition.

We test NUFVM on uniform trapezoidal meshes, Kershaw meshes, distorted quadrilateral meshes and Shestakov meshes, and the numerical results are shown in Tables 8-12. As shown in Tables 8-10, the convergence rate of NUFVM is $\mathcal{O}(h)$ in H^1 semi-norm, and $\mathcal{O}(h^2)$ in L^2 norm on four kinds of meshes. In addition, we test Shestakov meshes with distortion ranges $2/5$ and $4/9$. Tables 11-12 show that the convergence rate gradually decreases when the distortion range approaches $1/2$. However, the convergence rate is close to $\mathcal{O}(h)$ in H^1 semi-norm, and close to $\mathcal{O}(h^2)$ in L^2 norm. The numerical results

Table 8: Convergence rate for Example 5.5 on uniform trapezoidal meshes.

D	h	$ u - u_h _1$	Rate	$\ u - u_h\ _0$	Rate
1	$1/2^5$	8.2488×10^{-2}	-	6.2403×10^{-4}	-
	$1/2^6$	4.1256×10^{-2}	0.9999	1.5498×10^{-4}	2.0096
	$1/2^7$	2.0630×10^{-2}	0.9999	3.8612×10^{-5}	2.0050
	$1/2^8$	1.0315×10^{-2}	1.0000	9.6361×10^{-6}	2.0025
	$1/2^9$	5.1575×10^{-3}	1.0000	2.4069×10^{-6}	2.0013
10^{-6}	$1/2^5$	8.8079×10^{-2}	-	1.0260×10^{-3}	-
	$1/2^6$	4.4152×10^{-2}	0.9963	2.4545×10^{-4}	2.0635
	$1/2^7$	2.2103×10^{-2}	0.9982	6.0099×10^{-5}	2.0300
	$1/2^8$	1.1058×10^{-2}	0.9992	1.4875×10^{-5}	2.0144
	$1/2^9$	5.5303×10^{-3}	0.9997	3.7008×10^{-6}	2.0070
10^{-8}	$1/2^5$	8.8080×10^{-2}	-	1.0260×10^{-3}	-
	$1/2^6$	4.4153×10^{-2}	0.9963	2.4545×10^{-4}	2.0635
	$1/2^7$	2.2104×10^{-2}	0.9982	6.0100×10^{-5}	2.0300
	$1/2^8$	1.1059×10^{-2}	0.9991	1.4876×10^{-5}	2.0144
	$1/2^9$	5.5312×10^{-3}	0.9997	3.7009×10^{-6}	2.0070

Table 9: Convergence rate for Example 5.5 on distorted quadrilateral meshes.

D	h	$ u - u_h _1$	Rate	$\ u - u_h\ _0$	Rate
1	$1/2^5$	7.2545×10^{-2}	-	5.3514×10^{-4}	-
	$1/2^6$	3.6523×10^{-2}	0.9901	1.3277×10^{-4}	2.0110
	$1/2^7$	1.8304×10^{-2}	0.9966	3.3034×10^{-5}	2.0068
	$1/2^8$	9.1589×10^{-3}	0.9989	8.2172×10^{-6}	2.0072
	$1/2^9$	4.5816×10^{-3}	0.9993	2.0542×10^{-6}	2.0001
10^{-6}	$1/2^5$	7.6210×10^{-2}	-	1.2316×10^{-3}	-
	$1/2^6$	3.8495×10^{-2}	0.9853	2.9536×10^{-4}	2.0599
	$1/2^7$	1.9287×10^{-2}	0.9971	7.4764×10^{-5}	1.9821
	$1/2^8$	9.6725×10^{-3}	0.9956	1.8475×10^{-5}	2.0168
	$1/2^9$	4.8452×10^{-3}	0.9973	4.6791×10^{-6}	1.9813
10^{-8}	$1/2^5$	7.6702×10^{-2}	-	1.1921×10^{-3}	-
	$1/2^6$	3.8547×10^{-2}	0.9927	3.0358×10^{-4}	1.9733
	$1/2^7$	1.9200×10^{-2}	1.0055	7.3326×10^{-5}	2.0497
	$1/2^8$	9.6784×10^{-3}	0.9883	1.8690×10^{-5}	1.9721
	$1/2^9$	4.8402×10^{-3}	0.9997	4.7709×10^{-6}	1.9699

Table 10: Convergence rate for Example 5.5 on Kershaw meshes.

D	h	$ u - u_h _1$	Rate	$\ u - u_h\ _0$	Rate
1	$1/(3 \times 2^5)$	8.8199×10^{-2}	-	1.1274×10^{-3}	-
	$1/(3 \times 2^6)$	4.4182×10^{-2}	0.9973	2.8427×10^{-4}	1.9877
	$1/(3 \times 2^7)$	2.2102×10^{-2}	0.9993	7.1134×10^{-5}	1.9987
	$1/(3 \times 2^8)$	1.1052×10^{-2}	0.9998	1.7776×10^{-5}	2.0006
	$1/(3 \times 2^9)$	5.5263×10^{-3}	1.0000	4.4422×10^{-6}	2.0006
10^{-6}	$1/(3 \times 2^5)$	9.6981×10^{-2}	-	1.4079×10^{-3}	-
	$1/(3 \times 2^6)$	4.6245×10^{-2}	1.0684	3.5827×10^{-4}	1.9744
	$1/(3 \times 2^7)$	2.2595×10^{-2}	1.0333	9.0022×10^{-5}	1.9927
	$1/(3 \times 2^8)$	1.1172×10^{-2}	1.0161	2.2543×10^{-5}	1.9976
	$1/(3 \times 2^9)$	5.5558×10^{-3}	1.0079	5.6392×10^{-6}	1.9991
10^{-8}	$1/(3 \times 2^5)$	9.6986×10^{-2}	-	1.4080×10^{-3}	-
	$1/(3 \times 2^6)$	4.6248×10^{-2}	1.0684	3.5828×10^{-4}	1.9744
	$1/(3 \times 2^7)$	2.2596×10^{-2}	1.0333	9.0025×10^{-5}	1.9927
	$1/(3 \times 2^8)$	1.1173×10^{-2}	1.0161	2.2544×10^{-5}	1.9976
	$1/(3 \times 2^9)$	5.5560×10^{-3}	1.0079	5.6394×10^{-6}	1.9991

Table 11: Convergence rate for Example 5.5 on Shestakov meshes with distortion range 2/5.

D	h	$ u - u_h _1$	Rate	$\ u - u_h\ _0$	Rate
1	$1/2^5$	9.3238×10^{-2}	-	9.9724×10^{-4}	-
	$1/2^6$	5.0310×10^{-2}	0.8901	3.0324×10^{-4}	1.7175
	$1/2^7$	2.7258×10^{-2}	0.8842	9.2468×10^{-5}	1.7134
	$1/2^8$	1.4733×10^{-2}	0.8877	2.8399×10^{-5}	1.7031
	$1/2^9$	8.0019×10^{-3}	0.8806	8.7759×10^{-6}	1.6942
10^{-6}	$1/2^5$	1.0507×10^{-1}	-	2.3598×10^{-3}	-
	$1/2^6$	5.8643×10^{-2}	0.8414	7.6169×10^{-4}	1.6314
	$1/2^7$	3.2441×10^{-2}	0.8541	2.4418×10^{-4}	1.6413
	$1/2^8$	1.7681×10^{-2}	0.8756	7.7422×10^{-5}	1.6571
	$1/2^9$	9.8193×10^{-3}	0.8485	2.5402×10^{-5}	1.6078
10^{-8}	$1/2^5$	1.2381×10^{-1}	-	2.3117×10^{-3}	-
	$1/2^6$	6.8711×10^{-2}	0.8495	8.2965×10^{-4}	1.4784
	$1/2^7$	3.7788×10^{-2}	0.8626	2.8203×10^{-4}	1.5566
	$1/2^8$	2.0777×10^{-2}	0.8630	9.2422×10^{-5}	1.6095
	$1/2^9$	1.1554×10^{-2}	0.8466	3.0004×10^{-5}	1.6231

Table 12: Convergence rate for Example 5.5 on Shestakov meshes with distortion range 4/9.

D	h	$ u - u_h _1$	Rate	$\ u - u_h\ _0$	Rate
1	$1/2^5$	1.2059×10^{-1}	-	1.6907×10^{-3}	-
	$1/2^6$	6.6352×10^{-1}	0.8619	5.2225×10^{-4}	1.6948
	$1/2^7$	3.6440×10^{-2}	0.8646	1.6820×10^{-4}	1.6346
	$1/2^8$	2.0133×10^{-2}	0.8559	5.4390×10^{-5}	1.6288
	$1/2^9$	1.1125×10^{-2}	0.8558	1.7550×10^{-5}	1.6318
10^{-6}	$1/2^5$	1.4875×10^{-1}	-	4.0134×10^{-3}	-
	$1/2^6$	8.2770×10^{-2}	0.8457	1.3068×10^{-3}	1.6188
	$1/2^7$	4.6539×10^{-2}	0.8307	4.1946×10^{-4}	1.6394
	$1/2^8$	2.7006×10^{-2}	0.7852	1.4549×10^{-4}	1.5276
	$1/2^9$	1.5115×10^{-2}	0.8373	4.8110×10^{-5}	1.5965
10^{-8}	$1/2^5$	1.2096×10^{-1}	-	2.6776×10^{-3}	-
	$1/2^6$	6.9733×10^{-2}	0.7946	9.0094×10^{-4}	1.5715
	$1/2^7$	3.9170×10^{-2}	0.8321	3.2023×10^{-4}	1.4923
	$1/2^8$	2.1905×10^{-2}	0.8385	1.0838×10^{-4}	1.5630
	$1/2^9$	1.2291×10^{-2}	0.8336	3.6408×10^{-5}	1.5737

show that the convergence order is optimal even though the meshes do not satisfy $h^{1+\gamma}$ -parallelogram condition.

5.4 Boundary layer problem

In this part, we compare NUFVM with the finite volume element method(FVEM), whose definition is (2.18), and the standard upwind finite volume element method(SUFVM) in [29].

Example 5.6. In this part, we consider a convection-diffusion problem with boundary layers. Let the domain $\Omega = [0,1]^2$ and the convection velocity $\mathbf{b} = (2,3)^T$. The exact solution is chosen as

$$u(x,y) = e^{-\frac{(x-1)^2 + (y-1)^2}{0.02}}. \quad (5.10)$$

The source term f and the Dirichlet boundary value are given by the exact solution u . We take the scalar diffusion coefficient $\kappa(x,y) = D\mathbf{I}_2$, where D is constant and \mathbf{I}_2 is the identity matrix. Exact solution is shown in Fig. 7. We test our scheme on distorted quadrilateral meshes. From Table 13, we can see that the convergence rate of NUFVM is $\mathcal{O}(h)$ in H^1 semi-norm, and $\mathcal{O}(h^2)$ in L^2 norm. Table 14 shows that, FVEM leads to spurious oscillations when the convection is strongly dominant. As shown in Table 15, the convergence rate of SUFVM in L^2 norm is $\mathcal{O}(h)$. When the convection is strongly dominant, the convergence rate of SUFVM in H^1 norm is $\mathcal{O}(h^{\frac{1}{2}})$.

Table 13: Convergence rate of NUFVM for Example 5.6 on distorted quadrilateral meshes.

D	h	$ u - u_h _1$	Rate	$\ u - u_h\ _0$	Rate
1	$1/2^5$	1.0586×10^{-1}	-	1.1723×10^{-3}	-
	$1/2^6$	5.4023×10^{-2}	0.9705	3.0478×10^{-4}	1.9435
	$1/2^7$	2.6698×10^{-2}	1.0168	7.4285×10^{-5}	2.0366
	$1/2^8$	1.3442×10^{-2}	0.9900	1.8836×10^{-5}	1.9796
	$1/2^9$	6.7496×10^{-3}	0.9939	4.7436×10^{-6}	1.9895
10^{-6}	$1/2^5$	1.1524×10^{-1}	-	1.8802×10^{-3}	-
	$1/2^6$	5.8695×10^{-2}	0.9733	5.8708×10^{-4}	1.6793
	$1/2^7$	2.8686×10^{-2}	1.0329	1.5882×10^{-4}	1.8861
	$1/2^8$	1.4149×10^{-2}	1.0197	4.1615×10^{-5}	1.9323
	$1/2^9$	7.0762×10^{-3}	0.9996	1.0562×10^{-5}	1.9783
10^{-8}	$1/2^5$	1.1740×10^{-1}	-	1.9731×10^{-3}	-
	$1/2^6$	5.8475×10^{-2}	1.0055	6.0827×10^{-4}	1.6977
	$1/2^7$	2.8899×10^{-2}	1.0168	1.6096×10^{-4}	1.9180
	$1/2^8$	1.4214×10^{-2}	1.0237	4.1582×10^{-5}	1.9527
	$1/2^9$	7.0840×10^{-3}	1.0046	1.0675×10^{-5}	1.9617

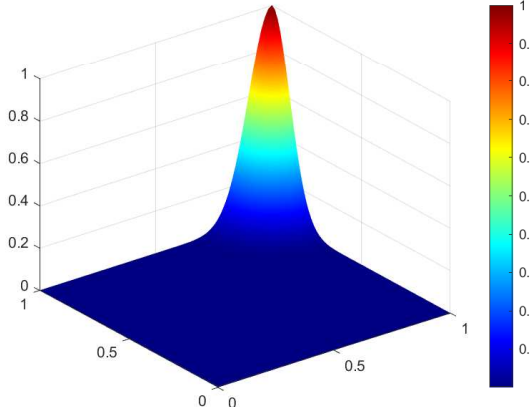


Figure 7: Exact solution for Example 5.6.

5.5 Three-dimensional problem

Example 5.7. In this part, we calculate our scheme on orthogonal-hexahedron meshes. We consider Eq. (1.1) with Dirichlet boundary condition on domain $\Omega = [0,1]^3$. We take the scalar diffusion coefficient $\kappa(x,y,z) = D\mathbf{I}_3$, where D is constant and \mathbf{I}_3 is the identity matrix. Take the constant convection velocity $\mathbf{b} = (3,2,1)^T$. The exact solution is chosen

Table 14: Convergence rate of FVEM for Example 5.6 on distorted quadrilateral meshes.

D	h	$ u - u_h _1$	Rate	$\ u - u_h\ _0$	Rate
1	$1/2^4$	1.9964×10^{-1}	-	4.0881×10^{-3}	-
	$1/2^5$	1.0170×10^{-1}	0.9731	1.0364×10^{-3}	1.9798
	$1/2^6$	5.3206×10^{-2}	0.9347	2.6831×10^{-4}	1.9497
	$1/2^7$	2.6791×10^{-2}	0.9898	6.8290×10^{-5}	1.9741
	$1/2^8$	1.3452×10^{-2}	0.9940	1.7187×10^{-5}	1.9904
	$1/2^9$	6.7506×10^{-3}	0.9947	4.3256×10^{-6}	1.9904
10^{-4}	$1/2^4$	7.0889×10^0	-	1.6641×10^{-1}	-
	$1/2^5$	5.9114×10^{-1}	3.5840	6.1207×10^{-3}	4.7649
	$1/2^6$	3.7146×10^{-1}	0.6703	1.4758×10^{-3}	2.0522
	$1/2^7$	1.2154×10^{-1}	1.6118	2.4357×10^{-4}	2.5991
	$1/2^8$	4.0597×10^{-2}	1.5820	4.1767×10^{-5}	2.5439
	$1/2^9$	1.4814×10^{-2}	1.4545	7.6353×10^{-6}	2.4516
10^{-6}	$1/2^4$	7.6922×10^1	-	1.8421×10^0	-
	$1/2^5$	5.0880×10^0	3.9182	5.9749×10^{-2}	4.9463
	$1/2^6$	7.7929×10^0	-0.6151	4.4990×10^{-2}	0.4093
	$1/2^7$	2.3237×10^0	1.7457	6.3962×10^{-3}	2.8143
	$1/2^8$	3.0252×10^0	-0.3806	4.3164×10^{-3}	0.5674
	$1/2^9$	2.9222×10^0	0.0500	1.9804×10^{-3}	1.1240
10^{-8}	$1/2^4$	5.5004×10^0	-	1.2876×10^1	-
	$1/2^5$	9.0618×10^0	-0.7203	1.0651×10^{-1}	0.2738
	$1/2^6$	3.6005×10^0	1.3316	2.0411×10^{-2}	2.3835
	$1/2^7$	2.9756×10^0	0.2750	8.5855×10^{-3}	1.2494
	$1/2^8$	3.2016×10^0	-0.1056	4.5333×10^{-3}	0.9213
	$1/2^9$	2.7833×10^0	0.2020	1.9302×10^{-3}	1.2318

to be

$$u(x, y, z) = 1 - e^{3x+2y+z-6/D} + e^{x+y+z}. \quad (5.11)$$

The source term f and the boundary value are set according to the exact solution u .

From Table 16, we can see that the convergence rate of NUFVM is $\mathcal{O}(h)$ in H^1 semi-norm, and $\mathcal{O}(h^2)$ in L^2 norm on orthogonal-hexahedron meshes.

We compare some finite volume methods for convection-diffusion problem on quadrilateral meshes including SUFVM, OWUFVM, CFS, GCFS and NUFVM. In Table 17, we list the cases about mesh condition, convergence order, whether these schemes can deal with anisotropic diffusion and whether these schemes have theoretical analysis. According to Table 17, we can see that the convergence rate in L^2 norm of SUFVM is only $\mathcal{O}(h)$, but the convergence rate in L^2 norm of other schemes are $\mathcal{O}(h^2)$. However, for second-

Table 15: Convergence rate of SUFVM for Example 5.6 on rectangular meshes.

D	h	$ u - u_h _1$	Rate	$\ u - u_h\ _0$	Rate
1	$1/2^5$	9.8350×10^{-2}	-	1.7094×10^{-3}	-
	$1/2^6$	4.9369×10^{-2}	0.9943	6.7733×10^{-4}	1.3355
	$1/2^7$	2.4728×10^{-2}	0.9977	3.0143×10^{-4}	1.1680
	$1/2^8$	1.2374×10^{-2}	0.9988	1.4281×10^{-4}	1.0778
	$1/2^9$	6.1894×10^{-3}	0.9994	6.9645×10^{-5}	1.0360
10^{-6}	$1/2^5$	1.7462×10^{-1}	-	6.0394×10^{-3}	-
	$1/2^6$	1.2588×10^{-1}	0.4722	3.1590×10^{-3}	0.9349
	$1/2^7$	9.2592×10^{-2}	0.4431	1.6326×10^{-3}	0.9523
	$1/2^8$	6.7291×10^{-2}	0.4605	8.3278×10^{-4}	0.9712
	$1/2^9$	4.8322×10^{-2}	0.4777	4.2098×10^{-4}	0.9842
10^{-8}	$1/2^5$	1.7462×10^{-1}	-	6.0394×10^{-3}	-
	$1/2^6$	1.2589×10^{-1}	0.4721	3.1591×10^{-3}	0.9349
	$1/2^7$	9.2596×10^{-2}	0.4431	1.6326×10^{-3}	0.9523
	$1/2^8$	6.7298×10^{-2}	0.4604	8.3278×10^{-4}	0.9712
	$1/2^9$	4.8332×10^{-2}	0.4776	4.2099×10^{-4}	0.9842

Table 16: Convergence rate of NUFVM for Example 5.7 on orthogonal-hexahedron meshes.

D	h	$ u - u_h _1$	Rate	$\ u - u_h\ _0$	Rate
1	$1/2^2$	6.5366×10^{-1}	-	8.8352×10^{-2}	-
	$1/2^3$	3.2473×10^{-1}	1.0093	2.1818×10^{-2}	2.0177
	$1/2^4$	1.6209×10^{-1}	1.0024	5.3752×10^{-3}	2.0212
	$1/2^5$	8.1014×10^{-2}	1.0006	1.3301×10^{-3}	2.0148
	$1/2^6$	4.0503×10^{-2}	1.0001	3.3056×10^{-4}	2.0086
10^{-6}	$1/2^2$	7.5181×10^{-1}	-	1.2031×10^{-1}	-
	$1/2^3$	3.7105×10^{-1}	1.0187	3.2370×10^{-2}	1.8940
	$1/2^4$	1.8324×10^{-1}	1.0179	8.4429×10^{-3}	1.9389
	$1/2^5$	9.0649×10^{-2}	1.0154	2.1631×10^{-3}	1.9646
	$1/2^6$	4.5001×10^{-2}	1.0103	5.4805×10^{-4}	1.9807
10^{-8}	$1/2^2$	7.5181×10^{-1}	-	1.2031×10^{-1}	-
	$1/2^3$	3.7105×10^{-1}	1.0187	3.2371×10^{-2}	1.8940
	$1/2^4$	1.8324×10^{-1}	1.0179	8.4429×10^{-3}	1.9389
	$1/2^5$	9.0649×10^{-2}	1.0154	2.1631×10^{-3}	1.9646
	$1/2^6$	4.5001×10^{-2}	1.0103	5.4806×10^{-4}	1.9807

Table 17: Comparison of five schemes.

	SUFVM	OWUFVM	CFS	GCFS	NUFVM
Rectangular meshes	✓	✓	✓	✓	✓
General quadrilateral meshes	✗	✗	✗	✗	✓
Anisotropic diffusion	✓	✗	✗	✓	✓
Convergence order in L^2 norm	1	2	2	2	2
Theoretical analysis	✓	✓	✗	✗	✓

order schemes, OWUFVM, CFS and GCFS are only defined on rectangular meshes, and OWUFVM and CFS can not deal with anisotropic Furthermore, CFS only has theoretical analysis in one-dimensional [44]. NUFVM not only can deal with anisotropic diffusion, but also has theoretical analysis on general quadrilateral meshes.

6 Conclusion

In this paper, we develop a new upwind finite volume element method for convection-diffusion-reaction problems on quadrilateral meshes. Firstly, in order to construct the upwind scheme, we use the two terms Taylor expansion to discrete the convection term. Secondly, we prove the coercivity, and establish the optimal error estimates in H^1 and L^2 norm respectively. We would like to point out that our scheme has optimal second-order convergence rate in L^2 norm, whether for dominant diffusion or for dominant convection. Numerical experiments confirm the theoretical results.

Acknowledgments

Y. Li was partially supported by the General Program of National Natural Science Foundation of China (No. 12071177). H. Yang was partially supported by the Youth Program of National Natural Science Foundation of China (No. 12301506). Y. Gao was partially supported by the LCP Fund for Young Scholar (No. 6142A05QN2101) and Zhejiang Provincial Natural Science Foundation of China (No. LQ24A010009).

References

- [1] A. N. Brooks, T. J. R. Hughes, Streamline upwind/Petrov-Galerkin formulations for convection dominated flows with particular emphasis on the incompressible Navier-Stokes equations, *Comput. Methods Appl. Mech. Engrg.*, 32 (1982), 199–259.
- [2] F. Brezzi, D. Marini, E. Süli, Residual-free bubbles for advection-diffusion problems: The general error analysis, *Numer. Math.*, 85 (2000), 31–47.
- [3] U. Kaya, M. Braack, Stabilizing the convection-diffusion-reaction equation via local problems, *Comput. Methods Appl. Mech. Engrg.*, 398 (2022), Paper No. 115243, 21.

- [4] T. Ikeda, Maximum Principle in Finite Element Models for Convection-Diffusion Phenomena, Kinokuniya Book Store Co., Ltd., Tokyo, 1983.
- [5] R. Eymard, T. Gallouët, R. Herbin, Finite Volume Methods, North-Holland, Amsterdam, 2000.
- [6] X. Meng, G. Hu, A NURBS-enhanced finite volume method for steady Euler equations with goal-oriented h -adaptivity, *Commun. Comput. Phys.*, 32 (2022), 490–523.
- [7] R. Li, Z. Chen, W. Wu, Generalized Difference Methods for Differential Equations: Numerical Analysis of Finite Volume Methods, Marcel Dekker, Inc., New York, 2000.
- [8] Z. Chen, R. Li, A. Zhou, A note on the optimal L^2 -estimate of the finite volume element method, *Adv. Comput. Math.*, 16 (2002), 291–303.
- [9] R. E. Ewing, T. Lin, Y. Lin, On the accuracy of the finite volume element method based on piecewise linear polynomials, *SIAM J. Numer. Anal.*, 39 (2002), 1865–1888.
- [10] Y. Li, R. Li, Generalized difference methods on arbitrary quadrilateral networks, *J. Comput. Math.*, 17 (1999), 653–672.
- [11] P. Chatzipantelidis, R. D. Lazarov, Error estimates for a finite volume element method for elliptic PDEs in nonconvex polygonal domains, *SIAM J. Numer. Anal.*, 42 (2005), 1932–1958.
- [12] P. Chatzipantelidis, V. Ginting, R. D. Lazarov, A finite volume element method for a nonlinear elliptic problem, *Numer. Linear Algebra Appl.*, 12 (2005), 515–546.
- [13] J. Lv, Y. Li, L^2 error estimate of the finite volume element methods on quadrilateral meshes, *Adv. Comput. Math.*, 33 (2010), 129–148.
- [14] J. Lv, Y. Li, L^2 error estimates and superconvergence of the finite volume element methods on quadrilateral meshes, *Adv. Comput. Math.*, 37 (2012), 393–416.
- [15] J. Lv, Y. Li, Optimal biquadratic finite volume element methods on quadrilateral meshes, *SIAM J. Numer. Anal.*, 50 (2012), 2379–2399.
- [16] Z. Chen, J. Wu, Y. Xu, Higher-order finite volume methods for elliptic boundary value problems, *Adv. Comput. Math.*, 37 (2012), 191–253.
- [17] M. Yang, J. Liu, Y. Lin, Quadratic finite-volume methods for elliptic and parabolic problems on quadrilateral meshes: Optimal-order errors based on Barlow points, *IMA J. Numer. Anal.*, 33 (2013), 1342–1364.
- [18] Z. Zhang, Q. Zou, Vertex-centered finite volume schemes of any order over quadrilateral meshes for elliptic boundary value problems, *Numer. Math.*, 130 (2015), 363–393.
- [19] Z. Chen, Y. Xu, Y. Zhang, A construction of higher-order finite volume methods, *Math. Comp.*, 84 (2015), 599–628.
- [20] Y. Lin, M. Yang, Q. Zou, L^2 error estimates for a class of any order finite volume schemes over quadrilateral meshes, *SIAM J. Numer. Anal.*, 53 (2015), 2030–2050.
- [21] M. Yang, J. Liu, Q. Zou, Unified analysis of higher-order finite volume methods for parabolic problems on quadrilateral meshes, *IMA J. Numer. Anal.*, 36 (2016), 872–896.
- [22] X. Wang, Y. Zhang, Z. Zhang, New superconvergent structures with optional superconvergent points for the finite volume element method, *Commun. Comput. Phys.*, 33 (2023), 1332–1356.
- [23] K. W. Morton, Numerical Solution of Convection-Diffusion Problems, Chapman & Hall, London, 1996.
- [24] R. D. Lazarov, I. D. Mishev, P. S. Vassilevski, Finite volume methods for convection-diffusion problems, *SIAM J. Numer. Anal.*, 33 (1996), 31–55.
- [25] T. Gallouët, R. Herbin, M. H. Vignal, Error estimates on the approximate finite volume solution of convection diffusion equations with general boundary conditions, *SIAM J. Numer. Anal.*, 37 (2000), 1935–1972.

- [26] T. Linss, Uniform pointwise convergence of an upwind finite volume method on layer-adapted meshes, *ZAMM Z. Angew. Math. Mech.*, 82 (2002), 247–254.
- [27] S.-H. Chou, D. Y. Kwak, P. S. Vassilevski, Mixed upwinding covolume methods on rectangular grids for convection-diffusion problems, *SIAM J. Sci. Comput.*, 21 (1999), 145–165.
- [28] I. D. Mishev, Finite volume element methods for non-definite problems, *Numer. Math.*, 83 (1999), 161–175.
- [29] D. Liang, Upwind generalized difference schemes for convection-diffusion equations, *Acta Math. Appl. Sinica*, 13 (1990), 456–466.
- [30] D. Liang, A kind of upwind schemes for convection diffusion equations, *Math. Numer. Sin.*, 13 (1991), 133–141.
- [31] P. Tamamidis, A new upwind scheme on triangular meshes using the finite volume method, *Comput. Methods Appl. Mech. Engrg.*, 124 (1995), 15–31.
- [32] E. Bertolazzi, G. Manzini, A cell-centered second-order accurate finite volume method for convection-diffusion problems on unstructured meshes, *Math. Models Methods Appl. Sci.*, 14 (2004), 1235–1260.
- [33] E. Bertolazzi, G. Manzini, A second-order maximum principle preserving finite volume method for steady convection-diffusion problems, *SIAM J. Numer. Anal.*, 43 (2005), 2172–2199.
- [34] S. Wang, G. Yuan, Y. Li, Z. Sheng, A monotone finite volume scheme for advection-diffusion equations on distorted meshes, *Internat. J. Numer. Methods Fluids*, 69 (2012), 1283–1298.
- [35] Q. Zhang, Z. Sheng, G. Yuan, A finite volume scheme preserving extremum principle for convection-diffusion equations on polygonal meshes, *Internat. J. Numer. Methods Fluids*, 84 (2017), 616–632.
- [36] N. T. Frink, Upwind scheme for solving the euler equations on unstructured tetrahedral meshes, *AIAA*, 30 (1992), 70–77.
- [37] B. Lan, Z. Sheng, G. Yuan, A monotone finite volume scheme with second order accuracy for convection-diffusion equations on deformed meshes, *Commun. Comput. Phys.*, 24 (2018), 1455–1476.
- [38] J. H. M. ten Thije Boonkkamp, M. J. H. Anthonissen, The finite volume-complete flux scheme for advection-diffusion-reaction equations, *J. Sci. Comput.*, 46 (2011), 47–70.
- [39] H. M. Cheng, J. H. M. ten Thije Boonkkamp, A generalised complete flux scheme for anisotropic advection-diffusion equations, *Adv. Comput. Math.*, 47 (2021), Paper No. 19, 26.
- [40] D. Liang, W. Zhao, An optimal weighted upwinding covolume method on non-standard grids for convection-diffusion problems in 2D, *Internat. J. Numer. Methods Engrg.*, 67 (2006), 553–577.
- [41] L. Ju, L. Tian, X. Xiao, W. Zhao, Covolume-upwind finite volume approximations for linear elliptic partial differential equations, *J. Comput. Phys.*, 231 (2012), 6097–6120.
- [42] Y. Gao, D. Liang, Y. Li, Optimal weighted upwind finite volume method for convection-diffusion equations in 2D, *J. Comput. Appl. Math.*, 359 (2019), 73–87.
- [43] P. G. Ciarlet, *The Finite Element Method for Elliptic Problems*, North-Holland Publishing Co., Amsterdam-New York-Oxford, 1978.
- [44] L. Liu, J. van Dijk, J. H. M. ten Thije Boonkkamp, D. B. Mihailova, J. J. A. M. van der Mullen, The complete flux scheme-error analysis and application to plasma simulation, *J. Comput. Appl. Math.*, 250 (2013), 229–243.
- [45] Q. Hong, J. Wu, Coercivity results of a modified Q_1 -finite volume element scheme for anisotropic diffusion problems, *Adv. Comput. Math.*, 44 (2018), 897–922.